Article

Neural circuitry for maternal oxytocin release induced by infant cries

https://doi.org/10.1038/s41586-023-06540-4

Received: 15 October 2021

Accepted: 15 August 2023

Published online: 20 September 2023

Check for updates

Silvana Valtcheva[1,2,3,4,5,7]✉, Habon A. Issa[1,2,3,4,5,7], Chloe J. Bair-Marshall[1,2,3,4,5], Kathleen A. Martin[1,2,3,4,5], Kanghoon Jung[6], Yiyao Zhang[2], Hyung-Bae Kwon[6] & Robert C. Froemke[1,2,3,4,5]✉

Oxytocin is a neuropeptide that is important for maternal physiology and childcare, including parturition and milk ejection during nursing[1–6]. Suckling triggers the release of oxytocin, but other sensory cues—specifically, infant cries—can increase the levels of oxytocin in new human mothers[7], which indicates that cries can activate hypothalamic oxytocin neurons. Here we describe a neural circuit that routes auditory information about infant vocalizations to mouse oxytocin neurons. We performed in vivo electrophysiological recordings and photometry from identified oxytocin neurons in awake maternal mice that were presented with pup calls. We found that oxytocin neurons responded to pup vocalizations, but not to pure tones, through input from the posterior intralaminar thalamus, and that repetitive thalamic stimulation induced lasting disinhibition of oxytocin neurons. This circuit gates central oxytocin release and maternal behaviour in response to calls, providing a mechanism for the integration of sensory cues from the offspring in maternal endocrine networks to ensure modulation of brain state for efficient parenting.

Parenting behaviours emerge from complex neural circuits that confer sensitivity to infant needs to ensure the survival of the species. One crucial molecular signal for the maternal brain is oxytocin, a nine-amino-acid peptide that is produced mainly in the paraventricular nucleus (PVN) and supraoptic nucleus of the hypothalamus[1–4]. Peripheral oxytocin is important for milk ejection during nursing and uterine contractions during labour, whereas oxytocin release in the central nervous system is involved in a wide range of behaviours including reproduction, parental care and pair bonding[5,6].

In humans, baby cries are a powerful signal of infant distress, and most nursing mothers respond to cries with increased hypothalamic activity, rises in the levels of plasma oxytocin, comforting behaviours towards the infant and occasional milk ejection[7,8]. Postpartum conditions might relate to lower levels of oxytocin and decreased sensitivity to infant cries[9], underscoring the importance of understanding the mechanisms by which acoustic stimuli from the offspring can activate oxytocin neurons. PVN oxytocin cells receive projections from many areas of the brain, but it is unknown which specific pathways relay auditory information and what synaptic mechanisms might mediate auditory responses and oxytocin release from oxytocin cells[3,10–15].

We made cell-attached and whole-cell recordings from PVN oxytocin neurons ($ChR2^+$, OT^+) and other optically unresponsive PVN neurons ($ChR2^-$, OT^-) in awake head-fixed mouse dams by using channelrhodopsin 2-assisted patching (Fig. 1a–c). Oxytocin neurons were identified by reliable spiking responses to brief pulses of blue light with comparable latencies to previous reports[13,14], and had baseline firing rates similar to those formerly described[13,14,16] (Extended Data Figs. 1 and 2a).

To investigate whether $ChR2^+$ (OT^+) and/or $ChR2^-$ (OT^-) neurons were activated by pup distress vocalizations, we measured one to two minutes of baseline spiking ('Pre') followed by repetitive presentation of a set of 15–18 distress calls recorded from isolated pups ('Calls'; each one-second call followed by one second of silence for a total duration of around 30–40 s), and assessed changes in ongoing activity thereafter for the duration of the recordings ('Post'). We found that pup-call presentation increased the firing rates of $ChR2^+$ (OT^+) neurons (Pre: 2.9 ± 0.7 Hz; Post: 5.0 ± 1.6 Hz; $P = 0.001$, $n = 11$ cells from $N = 6$ dams), but not those of $ChR2^-$ (OT^-) neurons (Pre: 3.1 ± 0.9 Hz, Post: 3.6 ± 1.0 Hz; $P = 0.07$, $n = 11$, $N = 5$; Fig. 1d–h and Extended Data Fig. 2b–f). This increase in the spiking of $ChR2^+$ (OT^+) neurons was not observed during call presentation itself (Extended Data Fig. 2g–j). To examine whether population-level activity was also enhanced after pup calls, we performed fibre photometry of oxytocin neuronal responses in awake head-fixed Oxytocin:Cre dams that were injected with AAVDJ-CAG-FLEx-GCaMP6s in the PVN and implanted with an optical fibre above the PVN (Fig. 1i). We measured changes in GCaMP6s signals in oxytocin neurons while we played pup distress calls, and observed substantial responses after calls (Pre versus Calls: $P = 0.0048$; Pre versus Post: $P = 0.0179$, $N = 7$ dams; Fig. 1j,k,m and Extended Data Fig. 3a,i,j). This increase in activity was significant as early as 25 s from call onset ($P = 0.013$). The sustained increase in oxytocin-neuron firing was specific to pup calls, as PVN neurons did not respond to pure tones, adult calls or frequency-modulated down-sweeps that retained key spectrotemporal characteristics of pup vocalizations (Fig. 1l,n and Extended Data Fig. 3c,e,g,h,j,k). We also did not observe significant activation of oxytocin cells in virgin mice, consistent with our previous findings[14] (Extended Data Fig. 3b,d,f,j).

[1]Skirball Institute for Biomolecular Medicine, New York University School of Medicine, New York, NY, USA. [2]Neuroscience Institute, New York University School of Medicine, New York, NY, USA. [3]Department of Otolaryngology, New York University School of Medicine, New York, NY, USA. [4]Department of Neuroscience and Physiology, New York University School of Medicine, New York, NY, USA. [5]Center for Neural Science, New York University, New York, NY, USA. [6]Solomon H. Snyder Department of Neuroscience, Johns Hopkins University School of Medicine, Baltimore, MD, USA. [7]These authors contributed equally: Silvana Valtcheva, Habon A. Issa. ✉e-mail: silvana.valtcheva@uk-koeln.de; robert.froemke@med.nyu.edu

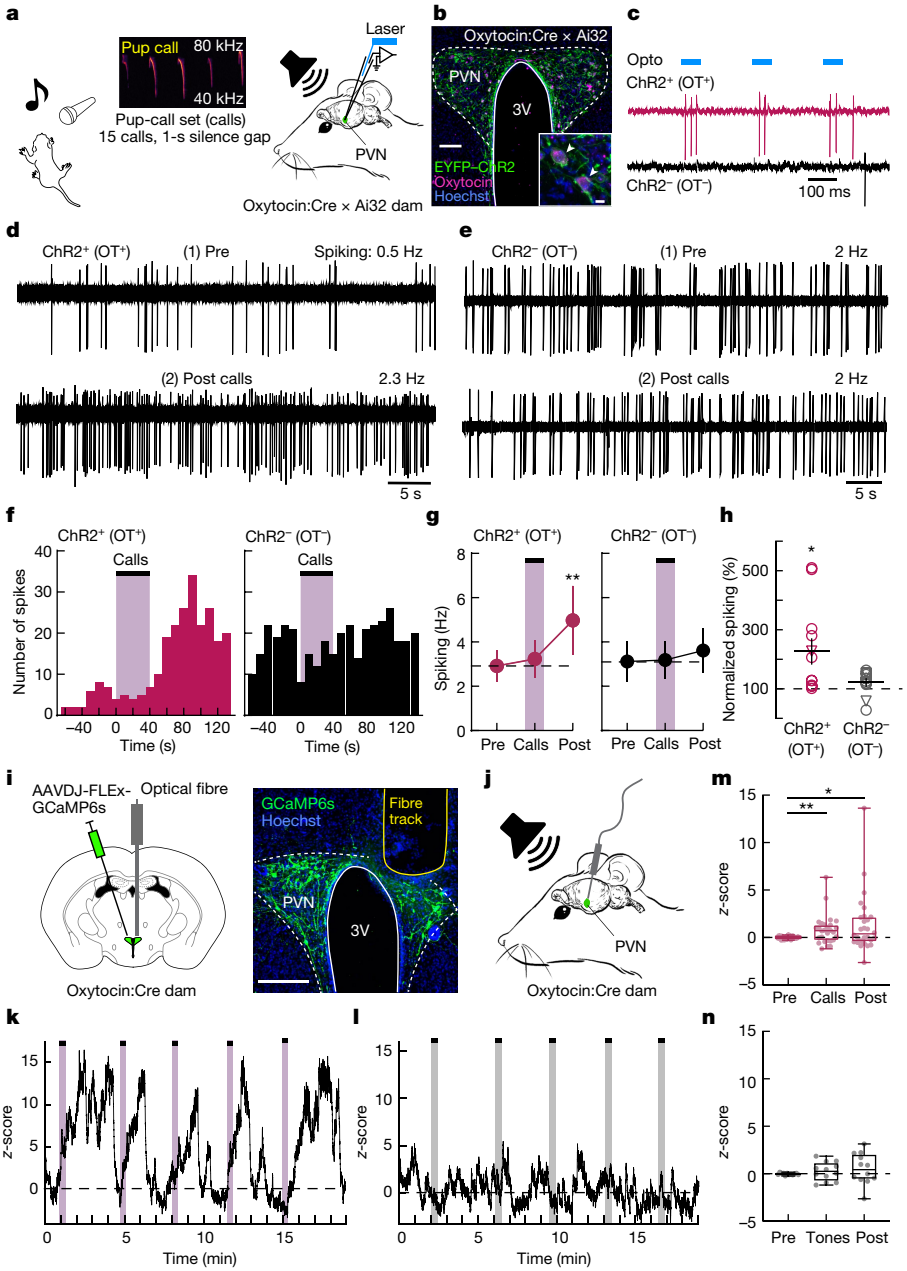

Fig. 1 | Delayed persistent activation of dam oxytocin neurons by pup vocalizations. a, In vivo cell-attached and whole-cell channelrhodopsin 2-assisted recordings and playback of pup calls. **b**, Oxytocin cells expressed EYFP–ChR2 (white arrowheads). Scale bars, 100 µm (main); 10 µm (inset). 3V, third ventricle. **c**, In vivo optogenetic identification of ChR2$^+$ (OT$^+$) neurons with reliable spiking to blue-light pulses ('Opto'). **d**,**e**, Cell-attached recordings of ChR2$^+$ (OT$^+$) (**d**) and ChR2$^-$ (OT$^-$) (**e**) neurons before the onset of pup calls (1, 'Pre') and 80 s after call onset (2, 'Post'). **f**, Peristimulus time histograms for ChR2$^+$ (OT$^+$) and ChR2$^-$ (OT$^-$) neurons. Bins, 10 s. **g**, Firing rate of ChR2$^+$ (OT$^+$) ($n = 11$ neurons, $N = 6$ dams; $P = 0.0014$, Friedman test) and ChR2$^-$ (OT$^-$) ($n = 11$, $N = 5$; $P = 0.07$) neurons. **h**, Change in the firing rate of ChR2$^+$ (OT$^+$) ($n = 12$; $P = 0.01$, one-sample two-tailed Student's t-test) but not ChR2$^-$ (OT$^-$) ($n = 11$; $P = 0.12$) neurons. Cell-attached (circles) and whole-cell (triangles) recordings. **i**, Injection of AAVDJ-CAG-FLEx-GCaMP6s into the PVN of Oxytocin:Cre dams and fibre implantation. Scale, 200 µm. **j**, Fibre photometry in awake head-fixed dams and playback of pup calls through an ultrasonic speaker. **k**–**n**, Oxytocin neurons responded to pup calls but not pure tones. **k**,**l**, Example timelines of responses to five sets of pup calls (**k**) or ultrasound pure tones (**l**). **m**,**n**, Box plots (showing the median (line), second to third quartiles (box) and minimum to maximum values (whiskers)) of z-scores of fluorescence activity preceding the onset ('Pre') of pup calls (**m**) or tones (**n**), during auditory stimulus ('Calls' or 'Tones') and after ('Post') (**m**, $N = 7$ dams; Pre versus Calls: $P = 0.005$; Pre versus Post: $P = 0.018$; **n**, $N = 3$ dams, Pre versus Calls: $P = 0.21$; Pre versus Post: $P = 0.34$; Wilcoxon matched-pairs signed-rank one-tailed test and correction for multiple comparisons). Data reported as mean ± s.e.m. or median ± minimum to maximum (**m**,**n**). *$P < 0.05$, **$P < 0.01$.

These results show that pup vocalizations can activate PVN oxytocin neurons, but not with stimulus-locked responses such as those typically observed in the central auditory system including the auditory cortex[17–20]. Instead, oxytocin cells require more prolonged stimulus periods to increase activity, perhaps as might naturally occur before and during episodes of maternal care.

We next sought to identify the projections that relay information about pup calls to PVN oxytocin neurons. We used *Cre*-inducible, retrograde pseudotyped monosynaptic rabies virus to identify the inputs to oxytocin cells that might relay auditory input from pup calls to the hypothalamus (Fig. 2a,b). Consistent with the absence of phase-locked responses to auditory stimuli in PVN neurons, most auditory areas did

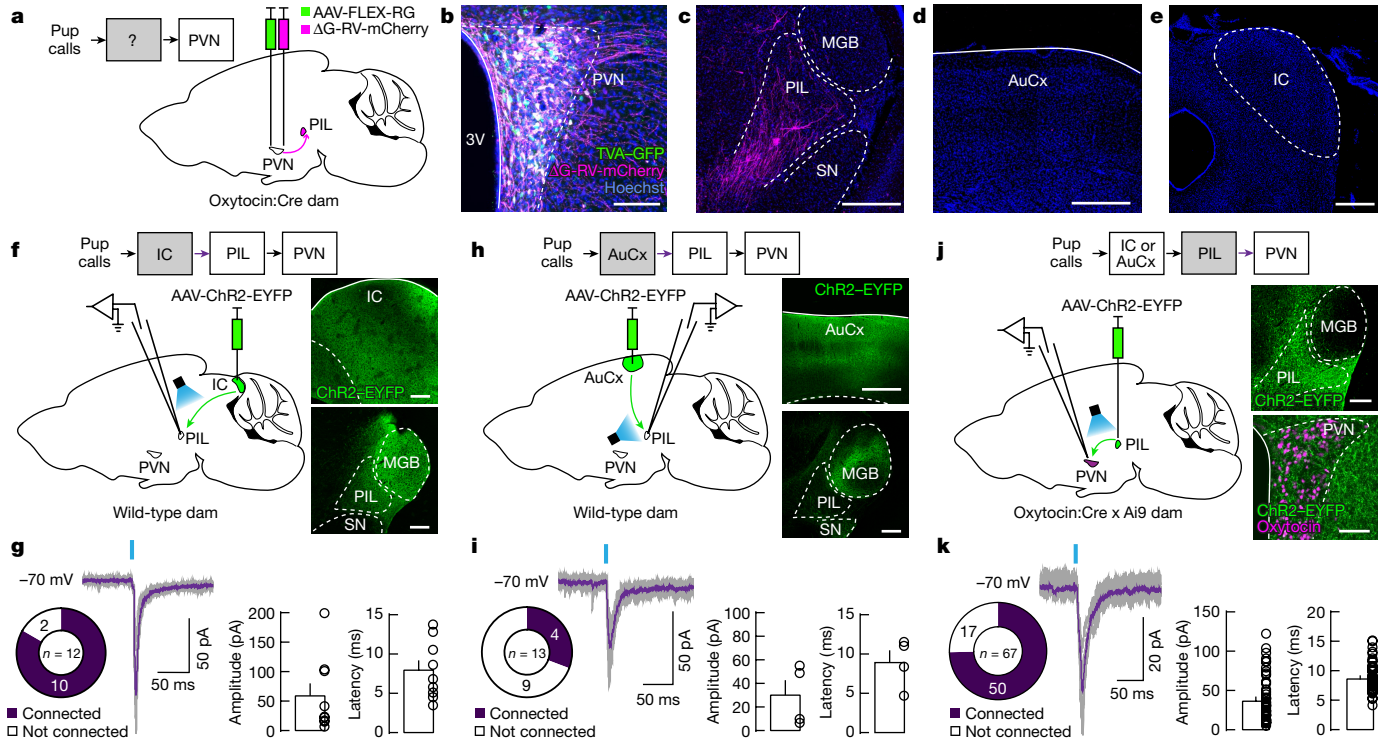

Fig. 2 | PVN oxytocin neurons receive projections from the auditory thalamus. **a**–**e**, Rabies-virus tracing. **a**, Injection of helper virus AAV2-EF1a-FLEX-TVA-GFP followed by *Cre*-inducible, retrograde pseudotyped monosynaptic rabies virus SADΔG-mCherry. **b**, Starter oxytocin neurons in the PVN expressing avian receptor protein (TVA)–GFP and glycoprotein-deleted rabies virus (ΔG-RV)–mCherry. Scale bar, 100 µm. **c**–**e**, Retrograde rabies infection and mCherry staining were absent in the MGB (**c**), AuCx (**d**) and IC (**e**). Dense rabies-infected field and robust expression of mCherry was found in the PIL (**c**; $N = 4$ dams). Scale bars, 500 µm. SN, substantia nigra. **f**,**g**, The PIL receives reliable input from the IC. **f**, Left, injection of AAV1-hSyn-hChR2(H134R)-EYFP into the IC of wild-type dams and whole-cell voltage-clamp recordings in PIL slices. Right, expression of ChR2–EYFP in the IC and IC projections in the MGB and the PIL. Scale bars, 200 µm. **g**, Characterization of oEPSCs in PIL neurons triggered by optogenetic stimulation of IC axons (10 out of 12 connected neurons, $N = 5$). **h**,**i**, The PIL receives sparser input from the AuCx. **h**, Left, injection of AAV1-hSyn-hChR2(H134R)-EYFP into the AuCx of wild-type dams and whole-cell voltage-clamp recordings in PIL slices. Right, expression of ChR2–EYFP in the AuCx and dense AuCx projections in the MGB but sparser projections in the PIL. Scale bars, 500 µm (top) and 200 µm (bottom). **i**, oEPSCs in PIL neurons triggered by optogenetic stimulation of AuCx axons (4 out of 13 connected neurons, $N = 3$). **j**,**k**, PVN oxytocin neurons receive reliable input from the PIL. **j**, Left, injection of AAV1-hSyn-hChR2(H134R)-EYFP into the PIL of Oxytocin:Cre × Ai9 dams and whole-cell voltage-clamp recordings from oxytocin neurons (tdTomato$^+$). Right, expression of ChR2–EYFP in the PIL and PIL projections in the PVN. Scale bars, 200 µm (top) and 100 µm (bottom). **k**, oEPSCs in oxytocin neurons triggered by optogenetic stimulation of PIL axons (50 out of 67 connected, $N = 21$). Data are mean ± s.e.m.

not send direct projections to the PVN. We did not detect retrograde rabies infection and mCherry staining in the medial geniculate body of the thalamus (MGB; Fig. 2c), the auditory cortex (AuCx; Fig. 2d) or the inferior colliculus (IC; Fig. 2e). Instead, we reliably observed dense rabies-based mCherry staining in the posterior intralaminar nucleus of the thalamus (PIL; Fig. 2c). The PIL contributed 100% to the auditory inputs in PVN oxytocin cells versus 0% for inputs from the MGB, AuCx and IC. The PIL is part of the nonlemniscal auditory pathway that projects to the PVN[13,21,22], and has also been implicated in maternal and social behaviours[22–24].

We found that the PIL is activated by pup calls. Even though firing rates of the PIL during pup calls and ultrasound pure tones are similar ($P = 0.33$), pure tones evoked only, transient activity for a duration of less than 50 ms, as previously described[25], compared to 1 s or more during pup calls (Extended Data Fig. 4). We then investigated whether the PIL receives functional synaptic inputs from the IC or AuCx, two major auditory areas that respond to pup calls. We tested the strengths of these synaptic connections using channelrhodopsin 2-assisted circuit mapping. We injected AAV1-hSyn-hChR2(H134R)-EYFP in the IC (Fig. 2f,g) or the AuCx (Fig. 2h,i) of wild-type dams, and performed whole-cell voltage-clamp recordings from PIL neurons in brain slices while optogenetically stimulating axons from either the IC or the AuCx. We found that the PIL receives synaptic inputs from both the IC and the AuCx, with a greater proportion of PIL neurons receiving inputs from the IC ($P = 0.015$, two-tailed Fisher's test; Fig. 2g,i). These findings are similar to those in other neurons in the paralaminar thalamus, which are more efficiently driven by inputs from the IC than those from the AuCx[26].

We then examined the strengths of synaptic connections between PIL and PVN oxytocin neurons[13,21,22]. We injected AAV1-hSyn-hChR2(H134R)-EYFP in the PIL of Oxytocin:Cre × Ai9 dams, to perform whole-cell voltage-clamp recordings from identified oxytocin neurons (expressing tdTomato) in PVN brain slices while optogenetically stimulating PIL terminals (Fig. 2j). We observed reliable optogenetically evoked excitatory postsynaptic currents (oEPSCs) in most oxytocin cells, indicating that oxytocin neurons receive connections from the PIL with a high probability (Fig. 2k). These monosynaptic connections were both excitatory[22] and inhibitory and preferentially targeted parvocellular oxytocin neurons (Extended Data Fig. 5a–h). Consistent with our rabies-virus tracing experiments, we did not observe axon terminals in the PVN originating from the IC or the AuCx (Extended Data Fig. 5i,j). These data reveal a noncanonical auditory circuit for relaying pup vocalization signals from the IC and the AuCx via the PIL to PVN oxytocin neurons.

The persistent activation of oxytocin neurons after pup calls could be due to several mechanisms: (1) long-term increases in PIL activity after pup calls; (2) changes in intrinsic excitability; or (3) synaptic plasticity.

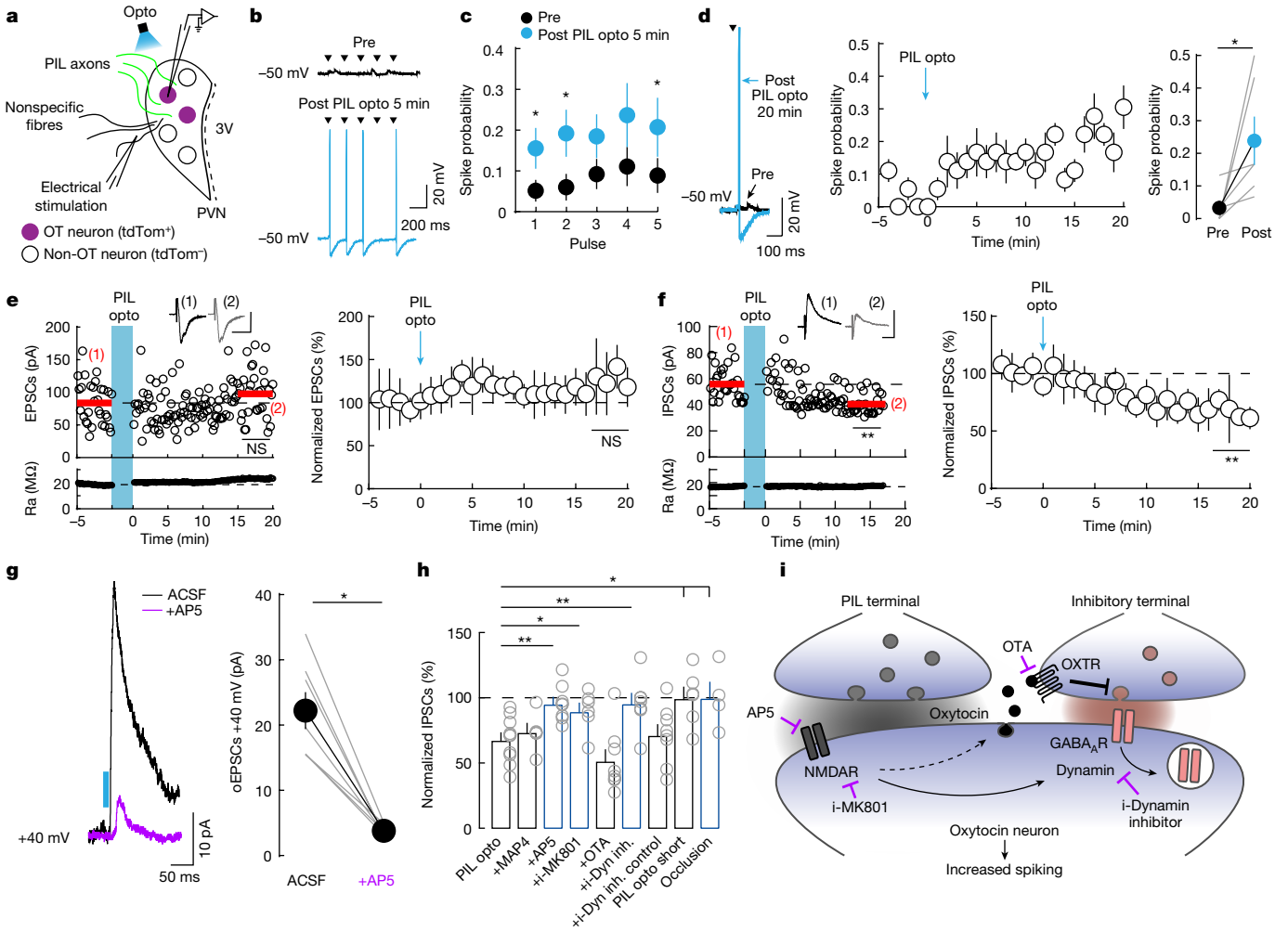

Fig. 3 | Activation of PIL–PVN inputs decreases inhibition in oxytocin neurons through postsynaptic NMDARs and the dynamin-dependent internalization of $GABA_A$Rs. a, Whole-cell recordings from tdTomato$^+$ oxytocin neurons in PVN slices, optogenetic stimulation of PIL axons and extracellular stimulation. **b**,**c**, Short-term enhanced spiking probability of oxytocin neurons after PIL opto. Improved spiking after 5-Hz electrical stimulation 5 min after PIL opto ('Post') versus baseline ('Pre'). **b**, Example. **c**, Summary ($n = 9$ neurons, pulses 1–5: $P = 0.016$, 0.023, 0.098, 0.094, 0.047, Wilcoxon matched-pairs signed-rank two-tailed test). **d**, Long-term enhanced spiking probability of oxytocin neurons after PIL opto after a single electrical stimulation pulse. Left, example. Middle, spiking probability ($n = 6$ neurons). Right, spiking significantly increased 20 min after PIL opto ($n = 6$; $P = 0.03$, Wilcoxon). **e**,**f**, PIL opto induced iLTD in oxytocin neurons. Ra, access resistance. **e**, No change in the magnitude of EPSCs after PIL opto. Left, example cell ($P = 0.15$, Mann–Whitney two-tailed test; scale bar, 20 ms and 50 pA). Right, summary ($n = 7$ neurons; $P = 0.14$, one-sample two-tailed Student's t-test). **f**, Decreased magnitude of IPSCs after PIL opto. Left, example cell ($P < 0.0001$, Mann–Whitney; scale bar, 20 ms and 100 pA). Right, summary ($n = 10$ neurons; $P = 0.0003$, one-sample Student's t-test). **g**, NMDAR-mediated currents in oxytocin cells with a single optogenetic stimulation pulse of PIL axons ($n = 7$ neurons; $P = 0.02$, Wilcoxon). **h**, iLTD is blocked by AP5 ($n = 8$; $P = 0.002$, Mann–Whitney), i-MK801 ($n = 6$; $P = 0.02$) and i-Dynamin inhibitor ($n = 7$; $P = 0.007$), and occluded by the presentation of pup calls ('Occlusion'; $n = 4$; $P = 0.014$), but not by MAP4 ($n = 5$; $P = 0.37$), OTA ($n = 8$; $P = 0.08$); PIL opto versus PIL opto short ($P = 0.02$), or PIL opto versus dynamin inhibitor control ($P = 0.90$). **i**, Possible mechanisms for postsynaptic NMDAR-dependent decreased inhibition. Data are mean ± s.e.m. (**c**,**d** (right), **g**,**h**) or mean ± s.d. (**d** (middle), **e**,**f**). *$P < 0.05$, **$P < 0.01$; NS, not significant.

We performed in vivo cell-attached recordings from PIL neurons in wild-type dams. Although we observed stimulus-evoked auditory responses in the PIL (Extended Data Fig. 4), pup calls did not trigger a long-term increase in spontaneous spiking (Extended Data Fig. 6). This makes it unlikely that the persistent activation of PVN oxytocin neurons resulted from increased PIL output after pup calls. We then asked whether the increased firing of PVN oxytocin neurons could be caused by changes in intrinsic excitability or synaptic plasticity mechanisms. We performed whole-cell current-clamp recordings from oxytocin neurons in PVN slices, and found that although PIL inputs to these cells occurred with high probability (Fig. 2k), these connections were too weak to trigger postsynaptic spiking responses (Extended Data Fig. 7a–c). We then used a stimulation pattern emulating PIL responses in vivo during pup-call playback by optogenetically stimulating PIL terminals in the PVN ('PIL opto') at 30 Hz for one second, and repeated this high-frequency activation every two seconds for three minutes. This stimulation pattern also did not elicit suprathreshold spiking in oxytocin cells (Extended Data Fig. 7d), possibly explaining why oxytocin neurons are not activated during individual pup calls in vivo (Extended Data Fig. 2h–j). There were no changes in the intrinsic properties of oxytocin neurons after PIL opto (Extended Data Fig. 7e–i), which indicates that the increased output of these cells in vivo is unlikely to be due to such a mechanism.

We observed a rapid and enduring increase in evoked spike generation in oxytocin neurons after PIL opto (Fig. 3a–d), similar to the persistent activity of oxytocin cells that we observed in vivo after pup calls. We investigated whether this repetitive PIL stimulation led to lasting changes in excitatory or inhibitory inputs onto oxytocin neurons,

particularly because the PVN is heavily innervated by various inhibitory inputs[27]. We monitored EPSCs and inhibitory postsynaptic currents (IPSCs) evoked by an extracellular stimulation electrode, before and after PIL opto (Fig. 3e,f). Although EPSCs were unaffected, the amplitudes of IPSCs were significantly decreased after PIL opto, without affecting PIL transmission itself (Extended Data Fig. 8a,b). Correspondingly, this long-term depression of inhibition (iLTD) decreased the IPSC/EPSC ratio for oxytocin neurons (Extended Data Fig. 8c). By contrast, emulating PIL responses in vivo during pure-tone playback by brief optogenetic stimulation of PIL terminals in the PVN ('PIL opto short') at 30 Hz for 100 ms repeated every two seconds for three minutes did not trigger iLTD (Extended Data Fig. 8d–f). In addition, iLTD was occluded in slices from dams that were exposed to pup-call playback immediately before the preparation of brain slices ('Occlusion'; Fig. 3h and Extended Data Fig. 8g–i), which suggests that disinhibition of oxytocin cells through iLTD occurs after pup calls in vivo.

Long-term reduction in inhibitory transmission can be mediated by different mechanisms. We first examined the involvement of type-III metabotropic glutamate receptors (mGluRs), which can be located on GABAergic terminals[28]. Activation of mGluRs was unlikely to produce the enhanced firing of oxytocin neurons after pup calls, because the type-III mGluR antagonist MAP4 did not prevent iLTD induction (Extended Data Fig. 9a). Next, we investigated whether iLTD relies on pre- or postsynaptic *N*-methyl-D-aspartate receptors (NMDARs). Optogenetic stimulation of PIL fibres activated NMDAR receptors on oxytocin neurons as it elicited outward oEPSCs, which were blocked by the NMDAR antagonist AP5 ($P = 0.02$; Fig. 3g). Furthermore, both bath application of AP5 and intracellular delivery of the use-dependent NMDAR blocker MK801 (i-MK801) through a recording pipette abolished iLTD after PIL opto (Extended Data Fig. 9b,c). These results show that iLTD of oxytocin neurons relied on postsynaptic NMDARs. Oxytocin release downstream of NMDAR activation[29] was not involved, because application of the oxytocin receptor (OXTR) antagonist OTA did not prevent iLTD (Extended Data Fig. 9d). NMDAR signalling can lead to a decrease in inhibitory transmission through Ca^{2+}-based signal transduction cascades[30]. In addition, NMDAR signalling can activate protein kinase C (PKC)[31], which is involved in dynamin phosphorylation and the dynamin-dependent internalization of postsynaptic γ-aminobutyric acid type A receptors ($GABA_A$Rs)[32]. Indeed, we found that iLTD and the change in the IPSC/EPSC ratio were blocked by infusing the postsynaptic oxytocin neuron with a membrane-impermeable dynamin inhibitory peptide (i-Dynamin inhibitor) through the recording pipette, but not by a scrambled dynamin inhibitor (i-Dynamin inhibitor control; Fig. 3h,i and Extended Data Fig. 9e,f). These findings suggest that PIL opto rapidly triggers iLTD in oxytocin neurons through postsynaptic NMDARs and dynamin signalling, possibly triggering the internalization of postsynaptic $GABA_A$Rs to decrease inhibitory transmission and increase spiking output.

Increased firing of oxytocin neurons triggered by auditory PIL input could have a substantial effect on maternal behaviour requiring the detection of pup calls[14,17–20,33]. Specifically, PIL lesions can impair pup-retrieval behaviour[34]. We asked whether chemogenetic suppression of PIL input to the PVN would affect the behavioural detection by dams of pup calls, as well as the execution of pup retrieval itself. We virally expressed the inhibitory hM4Di receptor, or mCherry as a control, in PVN-projecting PIL neurons, injecting wild-type dams with AAVrg-ENN.AAV.hSyn.Cre.WPRE.hGH in PVN and AAV8-hSyn-DIO-hM4D(Gi)-mCherry or AAV8-hSyn-DIO-mCherry in the PIL (Fig. 4a–e). To specifically test how the PIL-to-PVN pathway regulates the recognition of auditory cues related to pup distress, we tested approach behaviour towards a speaker playing pup calls in dams expressing hM4Di and administered intraperitoneally with either saline or clozapine *N*-oxide hydrochloride (CNO; Fig. 4f,g). Saline-injected dams needed 41.6 ± 5.9 played calls to approach the speaker—consistent with our observation that multiple pup calls were required to increase the activity of oxytocin cells (Fig. 4f)—and showed a significant preference for the speaker, compared to CNO-injected dams ($P = 0.002$; Fig. 4g).

We further tested pup-retrieval behaviour in dams expressing either hM4Di or mCherry control and injected intraperitoneally with saline or CNO using two different paradigms (Fig. 4h). As expected, control dams had lower latencies to approach an isolated crying pup than a speaker playing pup calls ($P < 0.0001$; Fig. 4i), probably owing to the multiple sensory cues from real pups. hM4Di dams were injected with either saline or CNO and allowed to remain undisturbed in the nest with their litter before being presented with only one pup at each trial for ten trials total. Overall, these dams had a decreased probability of retrieving at later trials, without changes in the time to retrieval (Fig. 4h,j–l). As expected, we did not observe this effect when CNO-injected hM4Di dams were presented with five isolated pups at the same time, without being previously in the nest (Fig. 4h,m). These results show that the PIL-to-PVN auditory input is important for sustaining maternal performance over time.

We hypothesized that if stimulating the PIL-to-PVN pathway leads to persistent activity of dam oxytocin neurons, then playing pup calls would lead to increased oxytocin release in brain areas that are involved in pup retrieval and maternal motivation[35,36]. Downstream oxytocin signalling specifically in the ventral tegmental area (VTA)[4,6,37,38] (Fig. 5a) has been shown to affect pup retrieval[39]. We found that infusing the OXTR antagonist OTA (0.5 mg ml^{-1}) into the VTA decreased the retrieval probability when dams were presented with five isolated pups at the same time (Extended Data Fig. 10). This effect is possibly because blocking oxytocin signalling in the VTA produces a more marked reduction of pup-retrieval behaviour than does selective chemogenetic inhibition of upstream PIL inputs to the PVN. We therefore hypothesized that PIL inputs to the PVN might mediate oxytocin release in the VTA in response to pup calls to ensure reliable pup-retrieval behaviour. We used a genetically encoded oxytocin sensor, *OXTR-iTango2* (refs. 40,41), to assess pup-call-triggered oxytocin release in the VTA of dams. This optogenetic system allows the detection of local endogenous oxytocin release, by using viral expression of OXTRs and then optically labelling those neurons after OXTR signalling (Fig. 5b). The *OXTR-iTango2* system requires two synthetic proteins, and their interaction causes the restoration of split TEV-protease function. Labelling neuronal populations with *OXTR-iTango2* consists of injecting three viral constructs into an area of interest: AAV1-hSYN-OXTR-TEV-C-P2A-iLiD-tTA (coding for the C-terminally truncated form of the OXTR; the N terminus of TEV protease; a blue-light-sensitive protein (AsLOV2); and tetracycline transactivator protein (tTA)); AAV1-hSYN-β-Arrestin2-TEV-N-P2A-TdTomato (coding for the protein β-arrestin 2 fused with the C terminus of the split TEV protease and tdTomato); and AAV1-hSYN-TRE-EGFP (coding for the tetracycline response element (TRE) and EGFP). Reconstitution of the TEV-protease N and C termini is ligand-dependent and occurs when oxytocin binds to the OXTR. Furthermore, recognition of the TEV cleavage site requires the presence of blue light. Thus, for *OXTR-iTango2*-labelled neuronal populations to detect endogenous oxytocin release, blue light is delivered via an optical fibre implanted in the same area. In the presence of oxytocin in the tissue, paired with blue-light illumination, the transactivation domain TRE can trigger the expression of EGFP. Detection of endogenously released oxytocin in the VTA of female and male mice during social interactions has been previously demonstrated using *OXTR-iTango2* (ref. 40).

We injected wild-type dams unilaterally in the left VTA with *OXTR-iTango2* viral constructs and implanted an optical fibre at the same site (Fig. 5c). Dams were exposed to blue-light illumination and pup calls ('Blue light + pup calls'), blue light and pure tones ('Blue light + tones') or blue light only ('Blue light only'). Auditory stimuli (pup calls or half-octave pure tones depending on the group) were paired with blue-light illumination delivered through the optical fibre connected to a blue laser (Fig. 5d). No auditory stimuli were presented to dams in the blue light only group. Cells expressing *OXTR-iTango2*

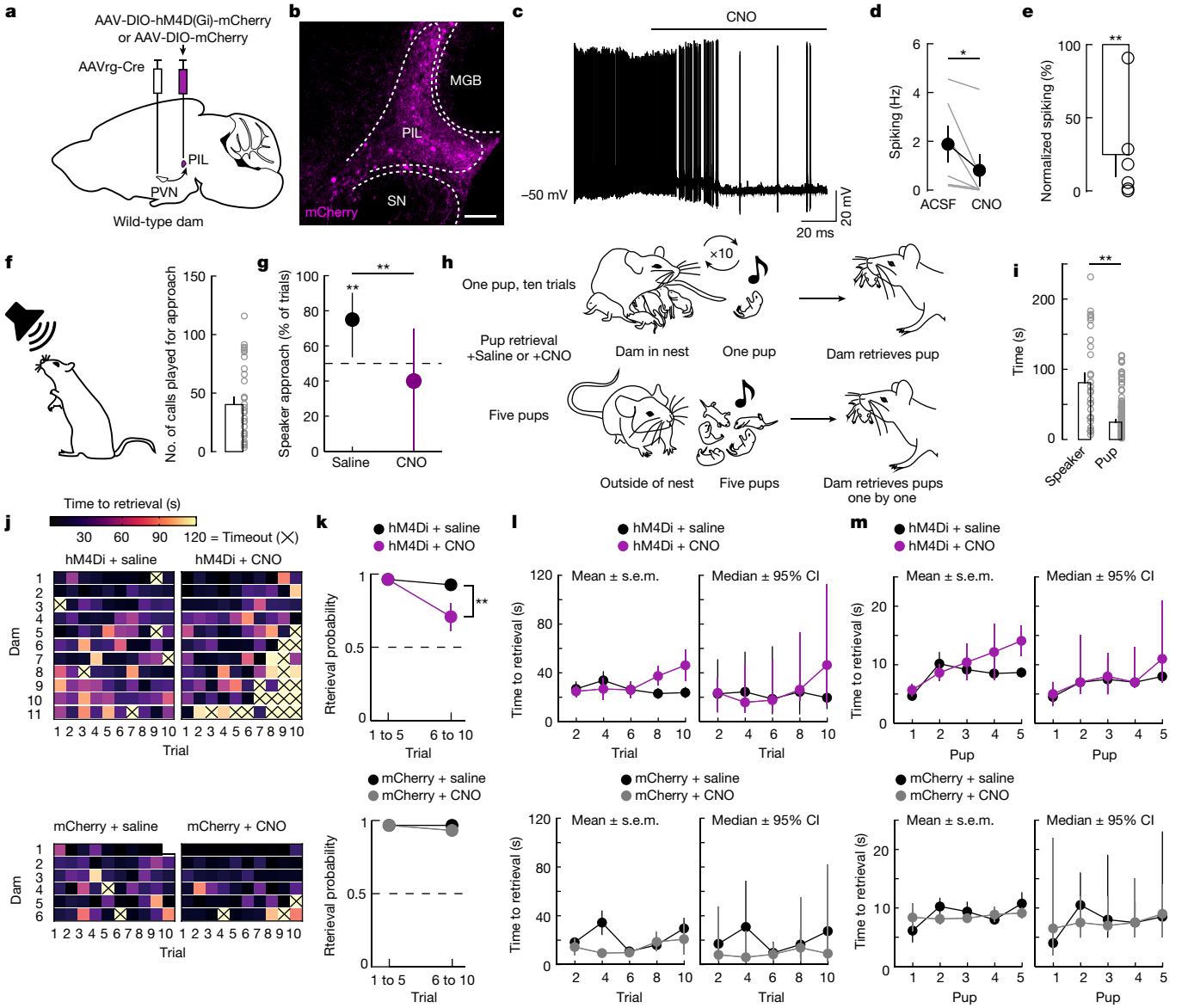

Fig. 4 | Chemogenetic inhibition of PIL projections to PVN impairs the detection of pup calls and pup-retrieval behaviour. a, Injection of AAVrg-ENN.AAV.hSyn.Cre.WPRE.hGH into the PVN and AAV8-hSyn-DIO-hM4D(Gi)-mCherry or AAV8-hSyn-DIO-mCherry into the PIL. **b**, Expression of mCherry in PVN-projecting PIL neurons. Scale bar, 200 µm. **c**–**e**, Bath application of CNO (1 µM) reduced the firing rate in PIL slices from dams expressing hM4Di. **c**, Example whole-cell current-clamp recording from a PIL neuron. **d**, Summary ($n = 6$ neurons; $P = 0.03$, Wilcoxon matched-pairs signed-rank two-tailed test). **e**, Normalized spiking for same neurons as in **d** ($P = 0.003$, one-sample two-tailed Student's t-test). **f**,**g**, Dams expressing hM4Di and injected with CNO had no preference for pup calls. **f**, Schematic of speaker approach protocol and number of calls played for approach (31 trials). **g**, Approach probability (43 trials; $N = 4$ dams; $P = 0.002$, two-tailed Fisher's test; two-tailed binomial test; saline: $P = 0.0054$, CNO: $P = 0.1173$). **h**–**m**, Dams expressing hM4Di and injected with CNO had impaired pup-retrieval behaviour. **h**, Pup-retrieval protocols. **i**, Latency to approach a speaker playing pup calls (31 trials) versus a crying pup (158 trials; $P < 0.0001$, Mann–Whitney two-tailed test). **j**–**l**, One pup, ten trials test. **j**, Performance of all dams across trials. **k**, Dams expressing hM4Di and injected with CNO retrieved with a lower probability compared to control saline-injected dams at trials 6 to 10 ($N = 11$ dams; $P = 0.0055$, Fisher's test); there was no difference in dams expressing mCherry ($N = 6$ dams; $P > 0.9999$, Fisher's test). **l**, No difference in time to retrieval for trials 6 to 10 (hM4Di: $N = 11$ dams; $P > 0.10$ for all, Mann–Whitney; mCherry: $N = 6$ dams, $P > 0.3939$, Mann–Whitney). **m**, Five pups test. No difference in time to retrieval (hM4Di: $N = 6$ dams; $P > 0.0556$, Mann–Whitney; mCherry: $N = 4$ dams, $P > 0.31$ for all, Mann–Whitney). Data are mean ± s.e.m. or median ± 95% confidence intervals (CI) (**g**; **l**,**m** as marked). $^*P < 0.05$, $^{**}P < 0.01$.

constructs in the VTA were labelled in red (tdTomato$^+$) and cells expressing the TRE–EGFP reporter signal were labelled in green (EGFP$^+$), marking neurons that responded to endogenously released oxytocin (Fig. 5e). There were many more tdTomato$^+$EGFP$^+$ cells in the VTA of the blue light + pup calls group compared to the blue light + tones or blue light only groups (Fig. 5f–h). Fewer tdTomato$^+$EGFP$^+$ cells were observed when the PIL-to-PVN pathway was inhibited with chemogenetics (Fig. 5i–k). This shows that the enhanced firing of PVN oxytocin neurons after pup calls can lead to central oxytocin release in downstream brain areas controlling pup retrieval such as the VTA, and that this effect is mediated by the activation of PIL inputs to the PVN.

Discussion

Here we define a noncanonical auditory circuit from the PIL to hypothalamic oxytocin neurons, which relays infant distress sounds to induce

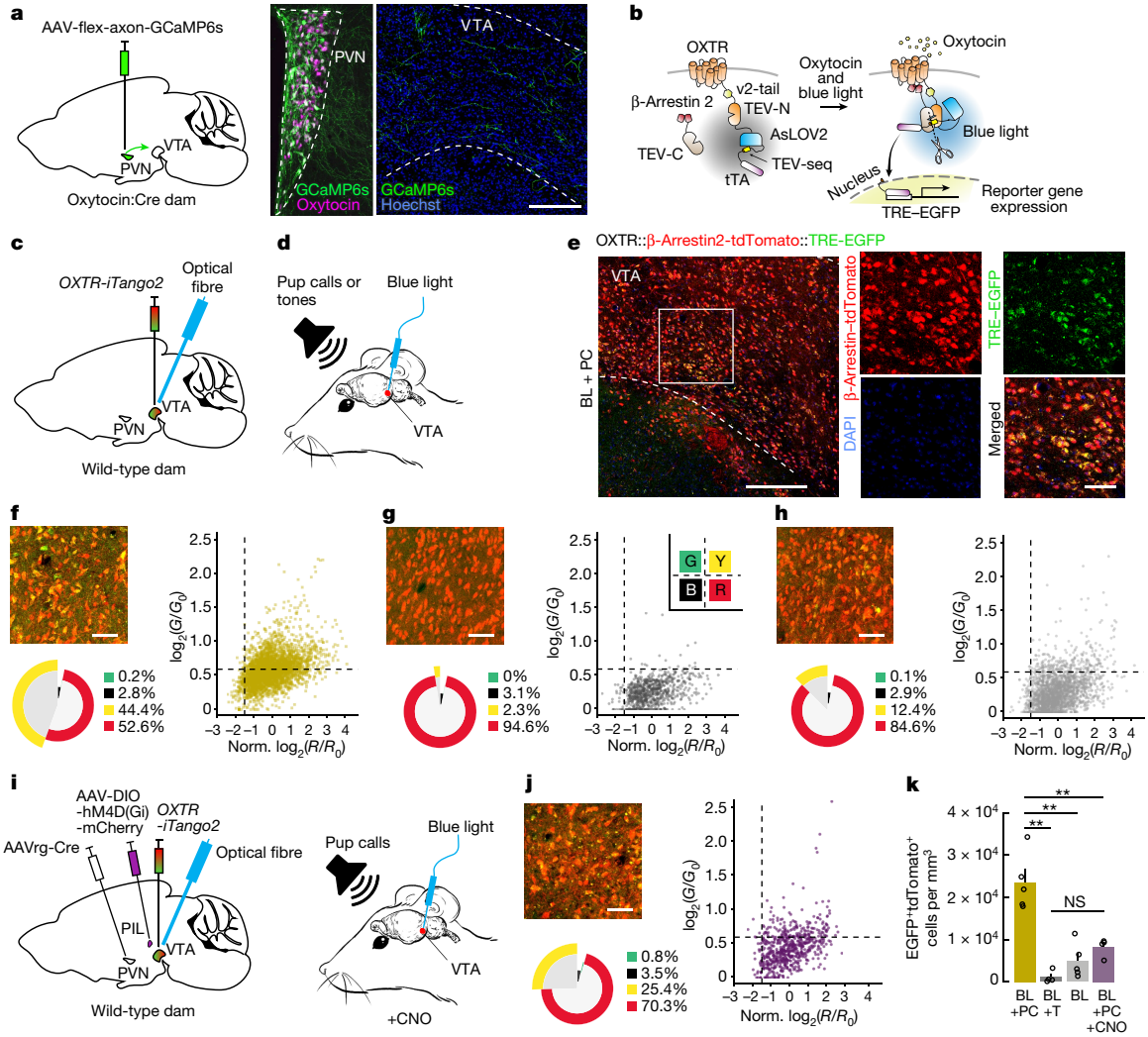

Fig. 5 | Pup calls trigger the release of oxytocin in the VTA through the PIL-to-PVN pathway. a, Injection of AAV5-hSynapsin1-FLEx-axon-GCaMP6s into the PVN of Oxytocin:Cre dams and GCaMP6s$^+$ axons in the VTA. Scale bar, 200 µm. $N = 2$ dams. **b**, Schematic of the *OXTR-iTango2* genetic strategy. TEV-seq, TEV protease cleavage recognition sequence; TEV-C, C terminus of TEV protease; TEV-N, N terminus of TEV protease; v2-tail, C-terminal tail of the vasopressin receptor 2. **c**, Injection of *OXTR-iTango2* viral constructs and fibre implantation in the VTA. **d**, Dams were exposed to pup calls paired with blue light ('Blue light + pup calls'; 'BL + PC'), pure tones paired with blue light ('Blue light + tones'; 'BL + T') or blue light alone ('Blue light only'; 'BL'). **e**, Images of VTA neurons expressing *OXTR-iTango2* constructs for the BL + PC group (left; scale bar, 200 µm) and magnified images from the area marked by a square (right; scale bar, 50 µm). **f**–**h**, Distribution patterns and percentage of *OXTR-iTango2*-labelled neurons in the VTA of dams (**f**, BL + PC; **g**, BL + T; **h**, BL). Scatter plots of individual cells (black dashed lines indicate threshold): cells with no viral infection (tdTomato$^-$EGFP$^-$; black, 'B'); cells with only a TRE-reporter signal (tdTomato$^-$EGFP$^+$; green, 'G'); cells with only a β-Arrestin–tdTomato signal (tdTomato$^+$EGFP$^-$; red, 'R'); and cells with both a red and a green signal (tdTomato$^+$EGFP$^+$; yellow, 'Y'). Average red (R) and green (G) fluorescent signals were calculated for each region of interest (ROI) and were divided by the mean background value ($R0$ and $G0$ for red and green channels, respectively) outside the ROIs for normalization. Scale bars, 50 µm. **i**, Injection of AAVrg-ENN.AAV.hSyn.Cre.WPRE.hGH into the PVN, AAV8-hSyn-DIO-hM4D(Gi)-mCherry into the PIL and *OXTR-iTango2* viral constructs into the VTA together with fibre implantation in the VTA. Dams were injected with CNO and exposed to pup calls paired with blue light (BL + PC + CNO). **j**, Distribution patterns and percentage of *OXTR-iTango2*-labelled neurons in the VTA of dams expressing hM4D(Gi) in PVN-projecting PIL cells and injected with CNO. Scale bar, 50 µm. **k**, Density quantification of *OXTR-iTango2*-labelled cells. There was a significant number of yellow (tdTomato$^+$EGFP$^+$) cells in the BL + PC group ($N = 5$) compared with the BL + T group ($N = 4$; $P < 0.0001$, one-way ANOVA; $P < 0.0001$, post hoc Bonferroni correction), BL group ($N = 5$; $P = 0.0001$), or BL + PC + CNO group ($N = 4$; $P = 0.0008$). There was no difference in the number of yellow cells between BL + T, BL and BL + PC + CNO. Data are mean ± s.e.m. $^{**}P < 0.01$; NS, not significant.

the release of oxytocin and affect maternal behaviour. This disinhibitory circuit provides a mechanistic understanding of how sensory cues from the offspring can be integrated into maternal endocrine networks for hormonal signalling. In dams, PVN oxytocin neurons showed delayed and long-lasting increases in firing after exposure to pup calls but not after exposure to pure tones, and PIL inputs onto parvocellular neurons controlled central oxytocin release and the efficiency of pup retrieval over time. Persistent activity seems to be a hallmark of hypothalamic neurons, which can be highly interconnected and have long integration periods[42–45]. Parvocellular neurons can also directly activate magnocellular neurons and have been proposed to operate as 'master cells' that control the activity of magnocellular cells and gate oxytocin release[1,13]. This would allow parvocellular neurons to regulate or control oxytocin release into different brain areas such as the VTA according to animal state and sensory experience.

Multiple calls over several seconds were required to activate oxytocin cells through disinhibition and to induce dams to approach the speaker. Hypothalamic inhibition increases during lactation[46] and might prevent the activation of oxytocin neurons by sparse synaptic

inputs, such as those occurring during single pup calls or during non-salient auditory stimuli such as pure tones. Our experiments indicate that a mechanism for the delayed oxytocin-neuron firing after pup calls could be a postsynaptic NMDAR-dependent decrease in inhibition. Oxytocin-neuron NMDARs can be activated without the need for postsynaptic spiking[47], suggesting that even if PIL inputs are too weak to trigger action potentials, prolonged subthreshold activation of oxytocin cells is sufficient to induce NMDAR-dependent inhibitory LTD. Postsynaptic NMDARs also regulate excitability[48,49] and trigger somatodendritic oxytocin release[47]. In turn, oxytocin signalling controls the probability of presynaptic GABA release through the postsynaptic release of endocannabinoids and the activation of presynaptic CB1 receptors[50]. Therefore, NMDARs can regulate synaptic inhibition in oxytocin cells by both pre- and postsynaptic mechanisms. Our findings provide a biological basis for the circuit and synaptic mechanisms that connect sensory cues from the offspring to the release of hormones in mothers. This circuit might promote plasticity and amplify neural representations across a broader range of infant cues to sustain maternal arousal and parental care over time.

Online content

Any methods, additional references, Nature Portfolio reporting summaries, source data, extended data, supplementary information, acknowledgements, peer review information; details of author contributions and competing interests; and statements of data and code availability are available at https://doi.org/10.1038/s41586-023-06540-4.

1. Althammer, F. & Grinevich,. Diversity of oxytocin neurons: beyond magno- and parvocellular cell types?. *J. Neuroendocrinol.* **30**, e12549 (2017).
2. Jurek, B. & Neumann, I. D. The oxytocin receptor: from intracellular signaling to behavior. *Physiol. Rev.* **98**, 1805–1908 (2018).
3. Valtcheva, S. & Froemke, R. C. Neuromodulation of maternal circuits by oxytocin. *Cell Tissue Res.* **1**, 57–68 (2019).
4. Froemke, R. C. & Young, L. J. Oxytocin modulation and neural plasticity. *Annu. Rev. Neurosci.* **8**, 359–381 (2021).
5. Dulac, C., O'Connell, L. & Wu, Z. Neural control of maternal and paternal behaviors. *Science* **345**, 1063–1069 (2014).
6. Dölen, G. Oxytocin: parallel processing in the social brain? *J. Neuroendocrinol.* **27**, 516–535 (2015).
7. McNeilly, A. S., Robinson, I. C., Houston, M. J. & Howie, P. W. Release of oxytocin and prolactin in response to suckling. *Br. Med. J.* **286**, 257–259 (1983).
8. Bornstein, M. H. et al. Neurobiology of culturally common maternal responses to infant cry. *Proc. Natl Acad. Sci. USA* **114**, E9465–E9473 (2017).
9. Pawluski, J. L., Lonstein, J. S. & Fleming, A. S. The neurobiology of postpartum anxiety and depression. *Trends Neurosci.* **40**, 106–120 (2017).
10. Grinevich, V. & Stoop, R. Interplay between oxytocin and sensory systems in the orchestration of socio-emotional behaviors. *Neuron* **99**, 887–904 (2018).
11. Chini, B., Verhage, M. & Grinevich, V. The action radius of oxytocin release in the mammalian CNS: From single vesicles to behavior. *Trends Pharmacol. Sci.* **11**, 982–991 (2017).
12. Resendez, S. L. et al. Social stimuli induce activation of oxytocin neurons within the paraventricular nucleus of the hypothalamus to promote social behavior in male mice. *J. Neurosci.* **40**, 2282–2295 (2020).
13. Tang, Y. et al. Social touch promotes interfemale communication via activation of parvocellular oxytocin neurons. *Nat. Neurosci.* **9**, 1125–1137 (2020).
14. Carcea, I. et al. Oxytocin neurons enable social transmission of maternal behaviour. *Nature* **596**, 553–557 (2021).
15. Yukinaga, H. et al. Recording and manipulation of the maternal oxytocin neural activities in mice. *Curr. Biol.* **32**, 3821–3829 (2022).
16. Wakerley, J. & Lincoln, D. The milk-ejection reflex of the rat: a 20- to 40-fold acceleration in the firing of paraventricular neurones during oxytocin release. *J. Endocrinol.* **3**, 477–493 (1973).
17. Cohen, L. & Mizrahi, A. Plasticity during motherhood: changes in excitatory and inhibitory layer 2/3 neurons in auditory cortex. *J. Neurosci.* **35**, 1806–1815 (2015).
18. Marlin, B. J., Mitre, M., D'Amour, J. A., Chao, M. V. & Froemke, R. C. Oxytocin enables maternal behaviour by balancing cortical inhibition. *Nature* **520**, 499–504 (2015).
19. Liu, R. C., Linden, J. F. & Schreiner, C. E. Improved cortical entrainment to infant communication calls in mothers compared with virgin mice. *Eur. J. Neurosci.* **23**, 3087–3097 (2006).
20. Tasaka, G. et al. The temporal association cortex plays a key role in auditory-driven maternal plasticity. *Neuron* **107**, 566–579 (2020).
21. Cai, D. et al. Distinct anatomical connectivity patterns differentiate subdivisions of the nonlemniscal auditory thalamus in mice. *Cereb. Cortex* **6**, 2437–2454 (2018).
22. Dobolyi, A., Cservenák, M. & Young, L. J. Thalamic integration of social stimuli regulating parental behavior and the oxytocin system. *Front. Neuroendocrinol.* **51**, 102–115 (2018).
23. Keller, D. et al. A thalamo-preoptic pathway promotes social grooming in rodents. *Curr. Biol.* **32**, 4593–4606 (2022).
24. Leithead, A. B., Godino, A., Barbier, M. & Harony-Nicolas, H. Social interaction elicits activity in glutamatergic neurons in the posterior intralaminar complex of the thalamus. *Biol. Psychiatry* https://doi.org/10.1016/j.biopsych.2023.05.016 (2023).
25. Bordi, F. & LeDoux, J. E. Response properties of single units in areas of rat auditory thalamus that project to the amygdala: II. Cells receiving convergent auditory and somatosensory inputs and cells antidromically activated by amygdala stimulation. *Exp. Brain Res.* **98**, 275–286 (1994).
26. Smith, P. H. et al. Cortical and collicular inputs to cells in the rat paralaminar thalamic nuclei adjacent to the medial geniculate body. *J. Neurophysiol.* **98**, 681–695 (2007).
27. Decavel, C. & van den Pol, A. GABA: a dominant neurotransmitter in the hypothalamus. *J. Comp. Neurol.* **302**, 1019–1037 (1990).
28. Piet, R., Vargová, L., Syková, E., Poulain, D. A. & Oliet, S. H. R. Physiological contribution of the astrocytic environment of neurons to intersynaptic crosstalk. *Proc. Natl Acad. Sci. USA* **101**, 2151–2155 (2004).
29. Brown, C. H., Ludwig, M., Tasker, J. G. & Stern, J. E. Somato-dendritic vasopressin and oxytocin secretion in endocrine and autonomic regulation. *J. Neuroendocrinol.* **32**, e12856 (2020).
30. Lu, Y. M., Mansuy, I. M., Kandel, E. R. & Roder, J. Calcineurin-mediated LTD of GABAergic inhibition underlies the increased excitability of CA1 neurons associated with LTP. *Neuron* **26**, 197–205 (2000).
31. Sun, L. & Liu, S. J. Activation of extrasynaptic NMDA receptors induces a PKC-dependent switch in AMPA receptor subtypes in mouse cerebellar stellate cells. *J. Physiol.* **2**, 537–553 (2007).
32. Robinson, P. J. et al. Dynamin GTPase regulated by protein kinase C phosphorylation in nerve terminals. *Nature* **365**, 163–166 (1993).
33. Schiavo, J. K. et al. Innate and plastic mechanisms for maternal behaviour in auditory cortex. *Nature* **587**, 426–431 (2020).
34. Factor, E. M., Mayer, A. D. & Rosenblatt, J. S. Peripeduncular nucleus lesions in the rat: I. Effects on maternal aggression, lactation, and maternal behavior during pre- and postpartum periods. *Behav. Neurosci.* **107**, 166–185 (1993).
35. Kohl, J. et al. Functional circuit architecture underlying parental behaviour. *Nature* **556**, 326–331 (2018).
36. Fang, Y.-Y., Yamaguchi, T., Song, S. C., Tritsch, N. X. & Lin, D. A hypothalamic midbrain pathway essential for driving maternal behaviors. *Neuron* **98**, 192–207 (2018).
37. Xiao, L. et al. Biased oxytocinergic modulation of midbrain dopamine systems. *Neuron* **95**, 368–384 (2017).
38. Hung, L. et al. Gating of social reward by oxytocin in the ventral tegmental area. *Science* **357**, 1406–1411 (2017).
39. Pedersen, C. A., Caldwell, J. D., Walker, C., Ayers, G. & Mason, G. A. Oxytocin activates the postpartum onset of rat maternal behavior in the ventral tegmental and medial preoptic areas. *Behav. Neurosci.* **108**, 1163–1171 (1994).
40. Mignocchi, N., Jung, K., Lee, D. & Kwon, H.-B. Development of a genetically-encoded oxytocin sensor. Preprint at *bioRxiv* https://doi.org/10.1101/2020.07.14.202598 (2020).
41. Lee, D. et al. Temporally precise labeling and control of neuromodulatory circuits in the mammalian brain. *Nat. Methods* **14**, 495–503 (2017).
42. Iremonger, K. J. & Bains, J. S. Integration of asynchronously released quanta prolongs the postsynaptic spike window. *J. Neurosci.* **27**, 6684–6691 (2007).
43. Branco, T. et al. Near-perfect synaptic integration by Nav1.7 in hypothalamic neurons regulates body weight. *Cell* **165**, 1749–1761 (2016).
44. Kennedy, A. et al. Stimulus-specific hypothalamic encoding of a persistent defensive state. *Nature* **586**, 730–734 (2020).
45. Daviu, N. et al. Paraventricular nucleus CRH neurons encode stress controllability and regulate defensive behavior selection. *Nat. Neurosci.* **23**, 398–410 (2020).
46. Giesl, U. & Theodosis, T. Synaptic plasticity in the rat supraoptic nucleus during lactation involves GABA innervation and oxytocin neurons: a quantitative immunocytochemical analysis. *J. Neurosci.* **5**, 2861–2869 (1994).
47. de Kock, C. P. J., Burnashev, N., Lodder, J. C., Mansvelder, H. D. & Brussaard, A. B. NMDA receptors induce somatodendritic secretion in hypothalamic neurones of lactating female rats. *J. Physiol.* **561**, 53–64 (2004).
48. Fleming, T. M. et al. State-dependent changes in astrocyte regulation of extrasynaptic NMDA receptor signalling in neurosecretory neurons. *J. Physiol.* **16**, 3929–3941 (2011).
49. Naskar, K. & Stern, J. E. A functional coupling between extrasynaptic NMDA receptors and A-type K+ channels under astrocyte control regulates hypothalamic neurosecretory neuronal activity. *J. Physiol.* **592**, 2813–2827 (2014).
50. Oliet, S. H. R., Baimoukhametova, D. V., Piet, R. & Bains, J. S. Retrograde regulation of GABA transmission by the tonic release of oxytocin and endocannabinoids governs postsynaptic firing. *J. Neurosci.* **27**, 1325–1333 (2007).

Methods

Mice

All procedures were approved under NYU School of Medicine Institutional Animal Care and Use Committee (IACUC) protocols, in accordance with National Institutes of Health (NIH) guidelines. Mice were housed in fully equipped facilities in the NYU School of Medicine Science Building. The facilities were operated by the NYU Division of Comparative Medicine. Mice were housed at around 22 °C, with a relative humidity of around 45%. The light cycle was 12 h on–12 h off (06:30–18:30 light). All experimental dams (0–3 weeks postpartum) had given birth for the first or second time and were housed with their own or foster pups (postnatal day (P) 0–P21), or were just weaned (less than one week after weaning). Surgeries were performed at 0–2 weeks postpartum in dams and more than 6 weeks of age in virgins. Dams were cohoused with younger pups (P1–P5) to maintain maternal behaviour after weaning of their own litter. Wild-type C57BL/6N (Taconic, B6-F) dams were used for in vivo and in vitro electrophysiology, anatomy tracings, oxytocin sensor experiments and behaviour. Oxytocin:Cre (Jackson, 024234) dams and virgins were used for anatomy tracings and fibre photometry. Oxytocin:Cre × Ai9 dams were used for in vitro electrophysiology and anatomy tracings. Oxytocin:Cre × Ai32 dams were used for in vivo electrophysiology and histology validation. Mice were maintained on a normal 12-h light–dark cycle (dark cycle starts at 18:00) and given food and water ad libitum. In vivo electrophysiology and behavioural experiments were performed at the end of the light cycle of the mice. Animals were randomly assigned to different groups. The investigators were blinded to allocation during behavioral testing, fiber photometry data analysis and oxytocin sensor data analysis. Blinding was not relevant and not performed for in vivo cell-attached, whole-cell and tungsten recordings, fiber photometry experiments, oxytocin sensor experiments and in vitro whole-cell recordings because auditory stimuli/optogenetic stimulation in vivo, and optogenetic/electrical stimulation and/or pharmacological application in vitro were performed in real time by the experimenter. Blinding was not relevant and not performed for data analysis of in vivo cell-attached, whole-cell and tungsten recordings, as well as for in vitro whole-cell recordings, because data analysis was performed in real time by the experimenter. No statistical methods were used to predetermine sample size. The experiments were not randomized. Sample sizes were chosen to reliably measure experimental effects while minimizing the number of animals used in accordance with ethical guidelines. Our sample sizes are comparable to those included in previous studies and were considered appropriate on the basis of the size and statistical significance of the effects and consistency across animals.

Stereotaxic surgery

Mice were anaesthetized with isoflurane (1–1.5%) and bilaterally injected with 400 nl (in the PVN) of AAV2-EF1a-FLEX-TVA-GFP (Salk Institute Viral Vector Core, 26197, titre: 2.73×10^{10} vg ml^{-1}), EnvA G-Deleted Rabies-mCherry (Salk Institute Viral Vector Core, 32636, titre: 3.78×10^{7} vg ml^{-1}) (ref. 51), AAVrg-ENN.AAV.hSyn.Cre.WPRE.hGH (Addgene, 105553-AAVrg, titre: 7×10^{12} vg ml^{-1}), AAV5-hSynapsin1-FLEx-axon-GCaMP6s (Addgene, 112010-AAV5, titre: at least 7×10^{12} vg ml^{-1}) or AAVDJ-CAG-FLEx-GCaMP6s (Penn Vector Core, V7340S, titre 3.2×10^{13}); 200 nl (in the PIL) of AAV8-hSyn-DIO-hM4D(Gi)-mCherry (Addgene, 44362-AAV8, titre: 1×10^{13} vg ml^{-1}) or AAV8-hSyn-DIO-mCherry (Addgene, 50459-AAV8, titre: 1×10^{13} vg ml^{-1}); 200 nl (in the PIL), 600 nl (in the AuCx) or 1 µl (in the IC) of AAV1-hSyn-hChR2(H134R)-EYFP (Addgene, 26973-AAV1, titre: 1×10^{13} vg ml^{-1}); and mice were unilaterally injected in the left hemisphere with 500 nl (in the VTA) of *OXTR-iTango2* viral constructs at a 1:1:2 ratio: AAV1-hSYN-OXTR-TEV-C-P2A-iLiD-tTA (titre: 2.1×10^{13} vg ml^{-1}), AAV1-hSYN-β-Arrestin2-TEV-N-P2A-TdTomato (titre: 2.57×10^{14} vg ml^{-1}) and AAV1-hSYN-TRE-EGFP (titre: 1.17×10^{13} vg ml^{-1}). Nanoject III (Drummond Scientific, 3-000-207) was used for AuCx, PIL, PVN and VTA injections. Pump 11 Elite Syringe Pump (Harvard Apparatus, HA1100) with a 5-µl Hamilton syringe, model 75 RN SYR (Hamilton Company, 7634-01) was used for IC injections. We waited two weeks after the injection of AAV2-EF1a-FLEX-TVA-GFP to inject EnvA G-Deleted Rabies-mCherry in the PVN. AAVrg-ENN.AAV.hSyn.Cre.WPRE.hGH (in the PVN) and AAV8-hSyn-DIO-hM4D(Gi)-mCherry or AAV8-hSyn-DIO-mCherry (in the PIL) were simultaneously injected. We used the following stereotaxic coordinates (in mm: AP, anteroposterior; ML, mediolateral; DV, dorsoventral): AuCx (−2.54 AP, +/−4.5 ML, −0.5 DV), IC (−5.2 AP, +/−1.5 ML, −1.5 DV), PIL (−2.7 AP, −1.7 ML, −3.7 DV), PVN (−0.72 AP, +/−0.12 ML, −4.7 DV) and VTA (−2.5 AP, +/−0.4 ML, −4 DV).

In vivo awake cell-attached and tungsten recordings

Oxytocin:Cre × Ai32 or wild-type dams were head-fixed using custom-made 3D-printed headposts and head-fixation frames. A small craniotomy (less than 1 mm) was performed over the sagittal sinus centred above the left PVN (coordinates in mm: −0.72 AP, −0.12 ML) in Oxytocin:Cre × Ai32 dams and above the left PIL (coordinates in mm: −2.7 AP, −1.7 ML) in wild-type dams. Cell-attached or whole-cell recordings from optically identified channelrhodopsin 2-expressing oxytocin neurons or other unidentified neurons were obtained from the PVN (4–5.2 mm below the pial surface). Cell-attached recordings using a conventional microelectrode holder or multiunit recordings with tungsten microelectrodes of PIL neurons in wild-type dams were obtained at 3.2–3.7 mm below the pial surface. Pipettes with a resistance of 5–6 MΩ and a long taper (around 6 mm) designed for subcortical recordings were made of borosilicate glass capillaries with an outer diameter of 1.5 mm and an inner diameter of 0.86 mm (Sutter Instruments, BF-150-86-10) using a P-87 micropipette puller (Sutter Instruments, P-87) and a 3 mm trough filament (Sutter Instruments, FT330B). Patch pipettes contained 127 mM potassium gluconate, 8 mM KCl, 10 mM phosphocreatine, 10 mM HEPES, 4 mM magnesium ATP and 0.3 mM sodium GTP (osmolality, 285 mOsm; pH 7.2 adjusted with KOH). The pressure of the patch pipette was monitored with a manometer (Omega, HHP680). A pressure of 15–20 mbar was applied when the patch pipette was lowered into the brain and the pressure was adjusted to 1.5–2 mbar when the pipette reached the targeted depth from the pial surface. Cell-attached recordings were obtained with a Multiclamp 700B amplifier (Molecular Devices) and data were acquired with Clampex 10.7 (Molecular Devices), low-pass filtered at 1 kHz, high-pass filtered at 100 Hz and digitized at 20 kHz. Multiunit recordings were obtained using tungsten microelectrodes (Microprobes for Life Science, WE30030.5A5) with a diameter of 2–3 µm and an impedance of 0.5 MΩ, connected to a DAM50 Extracellular Amplifier (World Precision Instruments); data were acquired with Clampex 10.7 (Molecular Devices), low-pass filtered at 3 kHz, high-pass filtered at 300 Hz and digitized at 100 kHz. The tip of the tungsten electrode was coated with DiI (Thermo Fisher Scientific, D282) for histological validation of the recording site.

In vivo optogenetic identification of PVN neurons

To identify channelrhodopsin 2-expressing PVN oxytocin neurons in Oxytocin:Cre × Ai32 dams through channelrhodopsin 2-assisted patching during each recording session[52,53], we used a Fiber-Optic Light Stimulating Device with a 465-nm blue LED (A-M Systems, 726500) connected to a Fiber-Optic Light Guide (A-M Systems, 726527). The optic fibre was inserted into the patch pipette using a 1.5-mm outer-diameter Continuous Optopatcher Holder (A-M Systems, 663943). Pulses of blue light were delivered through the optic fibre by a Digidata 1440A system (Molecular Devices) while recording in cell-attached or whole-cell configuration the responses of channelrhodopsin 2-positive oxytocin neurons (ChR2$^+$, OT$^+$) or other channelrhodopsin 2-negative PVN neurons (ChR2$^-$, OT$^-$). Different steps of light pulses (50 or 200 ms duration) were delivered with increasing intensity from 20 to 100% of the full LED power (3 mW at the tip of the fibre). ChR2$^+$ (OT$^+$) neurons

responded to light pulses by an increase in their firing rate and spiking probability, whereas ChR2$^-$ (OT$^-$) neurons were not modulated by blue light.

Fibre photometry

Oxytocin:Cre dams and virgins were bilaterally injected with AAVDJ-CAG-FLEx-GCaMP6s (Penn Vector Core, V7340S, titre 3.2×10^{13}) in PVN (coordinates in mm: −0.72 AP, +/−0.12 ML, −4.7 DV). Mice were head-posted and a 400-µm optical fibre (Thorlabs, CFMC54L05) was implanted in the left hemisphere slightly above the injection site at −4.5 D-V. Experiments were performed two to three weeks after surgery. Mice were placed in a head-fixation frame within a custom-built soundproof box and photometry was performed with a custom-built rig[14,54]. A 400-Hz sinusoidal blue light (40–45 µW) from a 470-nm LED (Thorlabs, M470F1) connected to a LED driver (Thorlabs, LEDD1B) was delivered through the optical fibre to excite GCaMP6s. We also used a control 330-Hz light (10 µW) from a 405-nm LED (Thorlabs, M405FP1) connected to a second LED driver. Light travelled through 405-nm and 469-nm excitation filters via a dichroic mirror to the brain. Emitted light travelled back through the same optical fibre via a dichroic mirror and 525-nm emission filter, passed through an adjustable zooming lens (Thorlabs, SM1NR05) and was detected by a femtowatt silicon photoreceiver (Newport, 2151). Recordings were performed using RX8 Multi-I/O Processor and Active X Software (Tucker-Davis Technologies). The envelopes of the signals were extracted in real time using Synapse software (Tucker-Davis Technologies). The analog readout was low-pass filtered at 10 Hz.

Auditory stimulation

Pup distress vocalizations were recorded from isolated pups aged P2–P8. Adult vocalizations were recorded during social interactions of male and female mice (more than 6 months old). Both pup and adult calls were recorded using an ultrasonic microphone (CM16/CMPA, Avisoft Bioacoustics, 41163, 200 kHz sampling rate; connected to an UltraSoundGate 116H recording interface, Avisoft Bioacoustics, 41163) and de-noised and matched in peak amplitude (Adobe Audition 23.3, Adobe) similarly to previous work[33]. To investigate responses to pup calls in individual oxytocin neurons, we monitored baseline firing rates for 1–2 min. For most cells (Fig. 1d–h and Extended Data Figs. 2b–g and 6c–e), we then played a set of pup calls consisting of 3–5 individual pup calls (with a duration of around 1 s for each call) repeated for a total of 15–18 calls with a 1-s delay between calls. Most calls were isolation or distress calls; for one neuron, wriggling calls were played. For the fibre photometry experiments (Fig. 1k,m and Extended Data Fig. 3a–d,i,j), we played 4 sets of pup or adult calls (pup calls: 5 calls; adult calls: 3 calls, for a total of 15 calls per set) separated by 1–3 min each. For the cells in Extended Data Fig. 2h–j and the multiunit recordings in Extended Data Fig. 4b,d–f, individual calls were played after 1-s baselines, with 3–6 different pup calls played for 10–15 times each. For studies of pure tones, half-octave (4–64 kHz) or ultrasound half-octave (23–64 kHz) 4 sets of pure tones (10-ms cosine ramp) at a sound pressure level (SPL) of 70 dB were played for 1 s (Fig. 1l,n and Extended Data Fig. 3e–g,j), in a pseudorandom order (repetition rate: 0.2 Hz, total of 15 tones per set, 3–4 sets). Frequency-modulated down-sweeps ('FM sweeps') that retained key spectrotemporal characteristics of pup vocalizations (72–30 kHz, 200-ms inter-syllable interval, 100-ms sweep duration, 0.2-Hz repetition rate, total of 15 sweeps per set, 3–4 sets) were played at 70 dB for 4 sets. For the cells in Extended Data Fig. 3k, and multiunit recordings in Extended Data Fig. 4c,f,g, 50-ms pure tones were played. All auditory stimuli were played using an RZ6 auditory processor (Tucker-Davis Technologies).

In vitro whole-cell recordings

Recordings in brain slices were conducted two to three weeks after virus injection. After being anaesthetized by isoflurane inhalation, mice were perfused with ice-cold sucrose-based cutting solution containing: 87 mM NaCl, 75 mM sucrose, 2.5 mM KCl, 1.25 mM NaH_2PO_4, 0.5 mM $CaCl_2$, 7 mM MgCl2, 25 mM $NaHCO_3$, 1.3 mM ascorbic acid and 10 mM D-glucose, bubbled with 95%/5% O_2/CO_2 (pH 7.4). The brain was rapidly placed in the same solution and 250-µm slices were prepared with a vibratome (Leica P-1000), placed in warm sucrose-based cutting solution bubbled with 95%/5% O_2/CO_2 (pH 7.4) and maintained at 33–35 °C for around 30 min, then cooled to room temperature (22–24 °C) for at least 1 h before use. For experiments, slices were transferred to the recording chamber and superfused (2.5–3 ml min^{-1}) with artificial cerebrospinal fluid (ACSF: 124 mM NaCl, 2.5 mM KCl, 1.5 mM $MgSO_4$, 1.25 mM NaH_2PO_4, 2.5 mM $CaCl_2$, 26 mM $NaHCO_3$ and 10 mM D-glucose) at 33 °C bubbled with 95%/5% O_2/CO_2 (pH 7.4). Neurons were identified with an Olympus 40× water-immersion objective with a TRITC filter. Pipettes with resistance 5–6 MΩ made of borosilicate glass capillaries with an outer diameter of 1.5 mm and an inner diameter of 0.86 mm (Sutter, BF-150-86-10) contained for voltage-clamp recordings: 130 mM caesium methanesulfonate, 1 mM QX-314, 4 mM TEA-Cl, 0.5 mM EGTA, 10 mM phosphocreatine, 10 mM HEPES, 4 mM magnesium ATP and 0.3 mM sodium GTP (osmolality, 285 mOsm; pH 7.2 adjusted with CsOH), or for current-clamp recordings: 127 mM potassium gluconate, 8 mM KCl, 10 mM phosphocreatine, 10 mM HEPES, 4 mM magnesium ATP and 0.3 mM sodium GTP (osmolality, 285 mOsm; pH 7.2 adjusted with KOH). Somatic whole-cell voltage-clamp and current-clamp recordings were made from PVN oxytocin neurons or PIL neurons with a Multiclamp 200B amplifier (Molecular Devices). Data were acquired with Clampex 10.7 (Molecular Devices), low-pass filtered at 2 kHz and digitized at 20 kHz. To measure the synaptic connectivity between areas using channelrhodopsin 2-assisted circuit mapping[55], whole-cell voltage-clamp recordings were made and neurons were held at −70 mV or 0 mV for EPSC or IPCS recordings, respectively. Channelrhodopsin 2-expressing axons were activated with 1-ms pulses of full field illumination with a 465-nm LED light (Mightex, SLC-AA02-US) repeated at 0.1 Hz. To measure NMDAR-mediated currents, whole-cell voltage-clamp recordings were made in the presence of picrotoxin (50 µM) and neurons were held at +40 mV. Amplitudes of NMDAR-mediated currents was measured 50 ms after optogenetic stimulation.

Long-term synaptic plasticity experiments

Whole-cell current-clamp or voltage-clamp recordings were made from PVN oxytocin neurons (red fluorescent) of Oxytocin:Cre × Ai9 dams injected with AAV1-hSyn-hChR2(H134R)-EYFP in the PIL. Action potentials or synaptic currents were evoked using an extracellular bipolar electrode made of 0.015 inch silver-chloride filament inserted into a borosilicate theta capillary glass with an outer diameter of 1.5 mm and an inner diameter of 1.00 mm (Warner Instruments, TG150-4) filled with ACSF and placed laterally and in close proximity to the PVN. To evoke action potentials or postsynaptic potentials in current-clamp mode, or synaptic currents in voltage-clamp mode, electrical pulses (0.1–10 mA and 0.1-ms duration) were delivered at 0.1 Hz with a Stimulus Isolator (World Precision Instruments, A365). Repeated optogenetic stimulation of PIL terminals in the PVN (PIL opto; 30 Hz during 1 s, repeated at 0.5 Hz for 3 min) was designed to mimic PIL discharge during pup-call presentation in vivo. Repeated brief optogenetic stimulation of PIL terminals in PVN (PIL opto short; 30 Hz during 100 ms, repeated at 0.5 Hz for 3 min) was designed to mimic PIL discharge during the presentation of pure tones in vivo. To examine the generation of action potentials, baselines were recorded for 2–5 min and the intensity of the electrical stimulation was tuned to remain mainly subthreshold; subthreshold activity or evoked action potentials were recorded for 5 min or 20 min after PIL opto. For monitoring synaptic currents, neurons were held at −70 mV for EPSCs and 0 mV for IPSCs. Neurons were held at −50 mV during PIL opto. After PIL opto or PIL opto short, synaptic currents were recorded for 15–20 min. For occlusion experiments, Oxytocin-Cre × Ai9 dams were exposed to

pup-call playback (3–5 individual pup calls of around 1-s duration per call, repeated for a total of 15 calls with a 1-s delay between calls), brains were immediately collected for preparation of PVN slices and synaptic plasticity recordings were obtained after 1 h of slice incubation. For excitability experiments, neurons were recorded in current-clamp configuration and held at around −50 mV (close to the resting membrane potential). The number of evoked spikes by different amplitudes of intracellular current injection was calculated before and after PIL opto. Recordings were excluded from analysis if the access resistance (Ra) changed by more than 30% compared to baseline. (d(CH_2)$_5^1$,Tyr(Me)^2,Thr^4,Orn^8,des-Gly-NH_2^9)-vasotocin trifluoroacetate salt (OTA; 1 μM; Bachem, 4031339), DL-2-amino-5-phosphono-pentanoic acid (AP5; 50 μM; Tocris, 0105), 4-aminopyridine (4-AP; 100 μM; Tocris, 0940), 6,7-dinitroquinoxaline-2,3-dione (DNQX; 25 μM; Tocris, 0189), (*S*)−2-amino-2-methyl-4-phosphonobutanoic acid (MAP4; 250 μM; Tocris, 0711), tetrodotoxin (TTX; 1 μM; Tocris, 1078) and CNO (1 μM; Millipore Sigma, SML2304) were dissolved directly in the extracellular solution and bath applied. Picrotoxin (50 μM; Millipore Sigma, P1675) was dissolved in ethanol and added to the extracellular solution, such that the final concentration of ethanol was 0.1%. Dizocilpine maleate (MK801; 1 mM; Tocris, 0924), dynamin inhibitory peptide, sequence QVPSRPNRAP (1.5 mM; Tocris, 1774) and dynamin inhibitory control peptide, sequence PRAPNSRQPV (50 μM; GenScript) were dissolved directly in the intracellular solution.

Chemogenetic inactivation

Wild-type dams were bilaterally injected with AAVrg-ENN.AAV.hSyn.Cre.WPRE.hGH in the PVN and with either AAV8-hSyn-DIO-hM4D(Gi)-mCherry or AAV8-hSyn-DIO-mCherry in the PIL. Approaches to the speaker broadcasting pup calls or pup-retrieval behaviour were measured at least three weeks after virus injection. One to two days before behaviour testing, dams were housed in a 26 × 34 × 18-cm cage with P1–P5 pups and nesting material. The day of behaviour testing, dams were intraperitoneally injected with 1 mg kg^{-1} CNO or the equivalent volume of saline, and pup-retrieval behaviour was measured.

For the approaches to the speaker broadcasting pup calls, dams were left in the cage and after verifying that the dam was in the nest with her litter for 1–2 min, the speaker was turned on and pup calls were played. The speaker was turned off after the dam approached the speaker and a pup was placed in front of the speaker to motivate dams for further trials. For pup-retrieval behaviour, two to four pups were left in the nest and the remaining pups were kept away from the cage and used for retrieval testing. An ultrasound microphone was used to verify that experimental pups were vocalizing before the start of the experiment. Retrieval of five pups: the dam was placed outside of the cage for 2 min, five pups were placed in the corner opposite to the nest and the dam was then reintroduced to the cage and placed in the empty nest. The dam was given two trials (2 min per trial) to retrieve all five pups and return them back to the nest. Retrieval of single pup: the dam was left undisturbed in the cage and after verifying that the dam was in the nest with her litter for 1–2 min, one pup was placed in the corner of the cage opposite to the nest. The dam was given ten trials (2 min per trial) to retrieve the displaced pup and return it back to the nest; if the displaced pup was not retrieved within 2 min, the pup was removed and the trial was scored as a failure. Another pup was then placed in an opposite corner and the next trial begun. If dams retrieved pups with 90% accuracy under saline conditions, they were injected with CNO and pup-retrieval behaviour was tested again after 30–40 min. Behavioural performance (probability of retrieving and time to retrieval) for each dam was compared between saline and CNO conditions. Each session of testing consisted of a baseline set (under saline injection) of two trials for five-pup retrieval and ten trials for single-pup retrieval, and a post-CNO injection set of two or ten trials, respectively. Experiments were performed under red light.

Cannula infusion

Wild-type dams were implanted with an infusion cannula (26 gauge, 5 mm, Plastics One, C315GAS-5/SPC) over the VTA. The day of the behavioural testing, 1 μl of the OXTR antagonist OTA (0.5 mg ml^{-1}) or an equal volume of saline was infused over 2 min with a Pump 11 Elite Syringe Pump (Harvard Apparatus, HA1100). The pup-retrieval test started 5 min after infusion. Behavioural testing was performed on different days for OTA and saline.

Oxytocin sensor

Wild-type dams were unilaterally injected in the left hemisphere with *OXTR-iTango2* (refs. 40,41) viral constructs (1:1:2 ratio; AAV1-hSYN-OXTR-TEV-C-P2A-iLiD-tTA, AAV1-hSYN-β-Arrestin2-TEV-N-P2A-TdTomato and AAV1-hSYN-TRE-EGFP) in VTA (coordinates in mm: −2.5 AP, −0.4 ML, −4 DV). A 200-μm optical fibre (Thorlabs, CFMXB05) was also implanted in the VTA using the same coordinates and a headpost was installed. In a subset of experiments, dams were also bilaterally injected with AAVrg-ENN.AAV.hSyn.Cre.WPRE.hGH in the PVN and with AAV8-hSyn-DIO-hM4D(Gi)-mCherry in the PIL. Pup calls, pure tones and blue-light exposure were performed three weeks after surgery. Dams were head-fixed during experiments. Mice in the blue light + pup calls group were exposed to pup calls (five different pup calls; duration of around 1 s; 0.5-Hz repetition rate; RZ6 auditory processor, Tucker-Davis Technologies) and paired with blue-light illumination (5 s ON–15 s OFF; DPSS Blue 473-nm laser, Opto Engine, MBL-F-473) for 45 min. Mice in the blue light + tones group were exposed to half-octave pure tones (ranging 4–64 kHz; 1-s duration, 10-ms cosine ramp, 70-dB SPL, 0.2-Hz repetition rate) played in a pseudorandom order with blue-light illumination (5 s ON–15 s OFF) for 45 min. Mice in the blue light only group were exposed to blue-light illumination only (5 s ON–15 s OFF) for 45 min. Mice in the blue light + pup calls + h4DM(Gi) + CNO group were injected with 1 mg kg^{-1} CNO 30 min before exposure to pup calls.

Histology and imaging

Mice were deeply anaesthetized with isoflurane inhalation followed by intraperitoneal injection (0.1 ml per 10 g) of a ketamine–xylazine mixture containing 15 mg ml^{-1} ketamine and 5 mg ml^{-1} xylazine, and transcardially perfused with phosphate-buffered saline (PBS) followed by 4% paraformaldehyde (PFA) in PBS. Brains were immersed overnight in 4% PFA followed by immersion in 30% sucrose for two nights. Brains were embedded with Tissue-Plus O.C.T. Compound medium (Thermo Fisher Scientific, 23-730) and sectioned at 50-μm thickness using a cryostat (Leica). After cryosectioning, brain sections were washed with PBS (3 × 10 min at room temperature) in a staining jar and incubated for 2 h at room temperature in blocking solution containing 5% normal goat serum (Millipore Sigma, G6767) in 1% Triton X-100 (Millipore Sigma, 11332481001) dissolved in PBS, followed by incubating for 48 h at room temperature with primary antibodies at 1:1,000 or 1:500 dilution in 3% normal goat serum in 1% Triton X-100 dissolved in PBS. Sections were washed with PBS (3 × 10 min at room temperature) and incubated for 2 h at room temperature in Alexa-Fluor-conjugated secondary antibodies diluted at 1:500 in PBS. After washing with PBS (2 × 10 min at room temperature), sections were incubated with Hoechst 33342 (Thermo Fisher Scientific, H3570) at 1:1,000 for nuclear staining. After washing with PBS (2 × 10 min at room temperature), slides were coverslipped using Fluoromount-G (SouthernBiotech). Slides were examined and imaged using a Carl Zeiss LSM 700 confocal microscope with four solid-state lasers (405/444, 488, 555 and 639 nm) and appropriate filter sets. Primary antibodies: GFP tag polyclonal antibody (Thermo Fisher Scientific, A10262), anti-mCherry antibody (Abcam, ab167453) and anti-oxytocin antibody (Millipore Sigma, AB911). Secondary antibodies: goat anti-rabbit IgG (H+L) cross-adsorbed secondary antibody, Alexa Fluor 555 (Thermo Fisher Scientific, A-21428) and goat

anti-chicken IgY (H+L) secondary antibody, Alexa Fluor 488 (Thermo Fisher Scientific, A-11039).

Electrophysiology

Off-line analysis was performed with Clampfit 10.7 (Molecular Devices). Spikes were automatically detected by threshold crossing. To investigate long-term responses to pup calls, the normalized firing rate was computed by calculating the percentage change in firing rate each minute. To investigate responses to individual pup calls, firing rate was measured throughout the call duration plus 300–400 ms, compared to spontaneous firing 1 s before call onset. To investigate responses to pure tones, the firing rate was measured 100 ms from the onset of the tone compared to the spontaneous rate 100 ms before tone onset. *Z*-scores were computed by calculating the call-evoked firing rate relative to the spontaneous firing rate: $z = (\mu_{evoked} - \mu_{spontaneous})/\sigma_{spontaneous}$ (ref. 18).

Fibre photometry

Data from both the 470 (signal) and the 405 (control) wavelength channels were independently filtered using a sliding window[56]. To normalize the scale of the control channel, a least-squares regression of the 470 and 405 wavelength channels was performed. Baseline corrections were estimated by subtracting the normalized control channel from the signal channel. The calculation of $\Delta F/F$ was carried out using the following equation: $(F - F_0)/F_0$, where F_0 represents the baseline signal detected by a first-order polynomial fitting. The analysis of all mice included the 'Pre' phase, which was defined as the 20 s before the onset of pup calls; the 'Calls' phase, which corresponded to the period of call playback; and the 'Post' phase, which covered the 20–40 s after call offset.

Oxytocin sensor

The *OXTR-iTango2*-labelled population in the VTA was categorized into four types on the basis of red and green fluorescent signals from post hoc data analysis of confocal imaging[40]. Individual regions of interest (ROIs) for cells were semi-automatically drawn using a custom algorithm (ImageJ 1.53t, NIH) on the basis of fluorescence intensity, cell size and cell shape. The average red (R) and green (G) fluorescent signals were calculated for each ROI and were divided by the mean background value (R_0 and G_0 for red and green channels, respectively) outside of the ROIs for normalization. ROIs were allocated into four different quadrants divided by thresholds in two fluorescent colours (*x* axis: red tdTomato signal, red threshold value: −1.5; *y* axis: green EGFP TRE-reporter signal, green threshold value: 0.585). ROIs with red signals above or below the red threshold value were categorized as tdTomato$^+$ or tdTomato$^-$, respectively. ROIs with green signals above or below the green threshold value were categorized as EGFP$^+$ or EGFP$^-$, respectively.

Statistics and reproducibility

Analysis of electrophysiology data was performed using Clampfit (Molecular Devices). Fibre photometry analysis was performed using MATLAB 2020b (MathWorks). Image analysis was conducted using ImageJ 1.53t (NIH). We used Wilcoxon matched-pairs signed-rank two-tailed test in Figs. 1m,n, 3c,d,g and 4d and Extended Data Figs. 1f, 2g,i, 3a–h, 4d, 5d,e and 7f–i. Friedman test was used in Fig. 1g. One-sample two-tailed Student's *t*-test was used in Figs. 1h, 3e,f and 4e and Extended Data Figs. 4e, 6e, 8b,c,e,f,h,i and 9a–f. Mann–Whitney two-tailed test was used in Figs. 3e,f,h, 4i,l,m and Extended Data Figs. 1g, 4f, 8d,g and 9a–f. One-way ANOVA was used in Fig. 5k and Extended Data Figs. 1b,d,e and 2j. Fisher's two-tailed test was used in Fig. 4g,k and Extended Data Fig. 10c. Two-tailed binomial test was used in Fig. 4g. All sample sizes and definitions as well precision measures (mean, s.e.m. or s.d.) are provided in the figure legends. Statistical tests and graph generation were performed using Prism 9.5.1 (GraphPad) or MATLAB 2020b (MathWorks).

Experiments were repeated independently with similar results for: $N = 6$ mice, Fig. 1b; $N = 7$, Fig. 1i; $N = 4$, Fig. 2b–e; $N = 27$, Fig. 4b; $N = 5$, Fig. 5e,f; $N = 4$, Fig. 5g; $N = 5$, Fig. 5h; $N = 4$, Fig. 5j; $N = 6$, Extended Data Fig. 4a.

Reporting summary

Further information on research design is available in the Nature Portfolio Reporting Summary linked to this article.

Data availability

Fibre photometry data are available on Zenodo: https://doi.org/10.5281/zenodo.8060338. Any updates to the above will be reflected in the NYU Data Catalog at https://datacatalog.med.nyu.edu/dataset/10623. Requests for further information about resources and reagents used and requests for data should be directed to and will be fulfilled by S.V. and R.C.F.

Code availability

Scripts used to analyse fibre photometry are available on GitHub: https://github.com/valtchevas/valtcheva_et_al_2023.

51. Wickersham, I. R., Finke, S., Conzelmann, K. & Callaway, E. M. Retrograde neuronal tracing with a deletion-mutant rabies virus. *Nat. Methods* **4**, 2006–2008 (2007).
52. Katz, Y., Yizhar, O., Staiger, J. & Lampl, I. Optopatcher—an electrode holder for simultaneous intracellular patch-clamp recording and optical manipulation. *J. Neurosci. Methods* **214**, 113–117 (2013).
53. Muñoz, W., Tremblay, R. & Rudy, B. Channelrhodopsin-assisted patching: in vivo recording of genetically and morphologically identified neurons throughout the brain. *Cell Rep.* **9**, 2304–2316 (2014).
54. Falkner, A. L., Grosenick, L., Davidson, T. J., Deisseroth, K. & Lin, D. Hypothalamic control of male aggression-seeking behavior. *Nat. Neurosci.* **19**, 596–604 (2016).
55. Petreanu, L., Huber, D., Sobczyk, A. & Svoboda, K. Channelrhodopsin-2-assisted circuit mapping of long-range callosal projections. *Nat. Neurosci.* **10**, 663–668 (2007).
56. Bruno, C. A. et al. pMAT: an open-source software suite for the analysis of fiber photometry data. *Pharmacol. Biochem. Behav.* **201**, 173093 (2021).

Acknowledgements We thank I. Carcea, E. Glennon, K. V. Kuchibhotla, J. K. Schiavo and S. C. Song for comments, discussions and technical assistance; the NYU Langone Microscopy Core for experimental and technical support; D. Rinberg for sharing the custom-made 3D-printed headpost and head-fixation frame design; and D. Lin for help with the code for analysing the fibre photometry data. Initial aliquots of the EnvA G-Deleted Rabies-mCherry (SADΔG-mCherry) and helper AAV2-EF1a-FLEX-TVA-GFP viruses were a gift from G. Fishell. Illustrations in Figs. 1a,j and 5d,i and Extended Data Figs. 4a, 6a and 10b were made by S. E. Ross. This work was funded by a Fyssen Foundation Postdoctoral Fellowship, a Leon Levy Foundation Postdoctoral Fellowship and a Brain & Behavior Research Foundation NARSAD Young Investigator Award (S.V.); a T32 MH019524 Training in Systems and Integrative Neuroscience award (H.A.I.); a Natural Sciences and Engineering Research Council of Canada PGS-D fellowship (C.J.B.-M.); an NSF Graduate Research Fellowship (K.A.M.); DP1MH119428 (H.-B.K.); the BRAIN Initiative (NS107616; Y.Z. and R.C.F.); and NINDS (NS074972), NICHD (HD088411), NIDCD (DC12557) and a Howard Hughes Medical Institute Faculty Scholarship (R.C.F.).

Author contributions S.V. performed in vivo cell-attached, whole-cell and tungsten recordings, fibre photometry, in vitro whole-cell recordings, behaviour for chemogenetic inactivation studies, oxytocin sensor experiments, viral injections, histology, image acquisition and data analysis of electrophysiology and behaviour experiments. H.A.I. performed fibre photometry and behaviour for chemogenetic inactivation and cannula infusion studies. C.J.B.-M. performed fibre photometry and in vitro whole-cell recordings for the scrambled dynamin inhibitor experiments. H.A.I., K.A.M. and Y.Z. wrote code and performed analysis of the photometry recordings. K.J. and H.-B.K. contributed to the design of viral constructs and data analysis for the oxytocin sensor. S.V. and R.C.F. designed the study and wrote the paper.

Competing interests The authors declare no competing interests.

Additional information

Supplementary information The online version contains supplementary material available at https://doi.org/10.1038/s41586-023-06540-4.

Correspondence and requests for materials should be addressed to Silvana Valtcheva or Robert C. Froemke.

Peer review information *Nature* thanks Cristina Marquez and the other, anonymous, reviewers for their contribution to the peer review of this work. Peer reviewer reports are available.

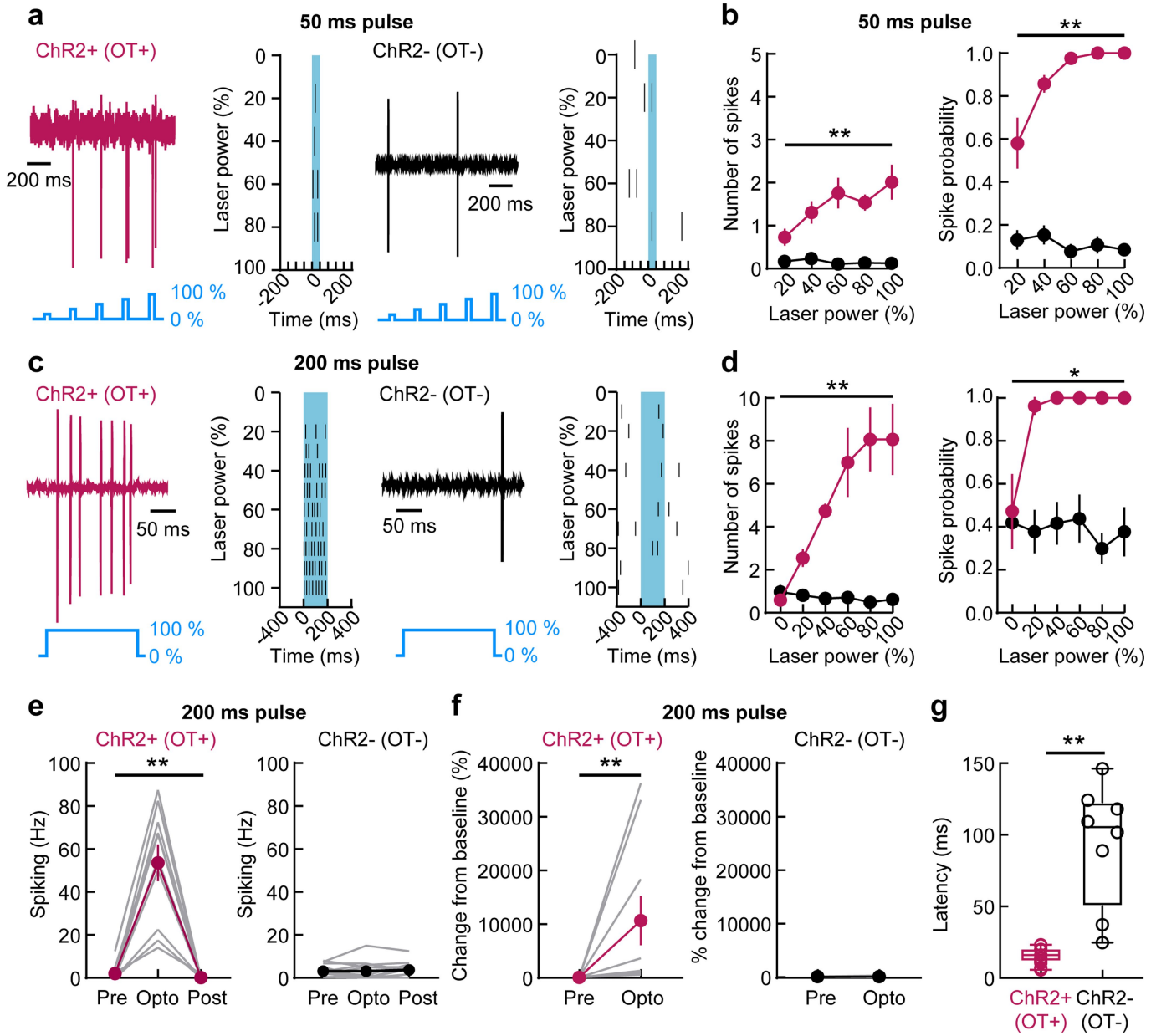

Extended Data Fig. 1 | Identification of ChR2$^+$ (OT$^+$) and ChR2$^-$ (OT$^-$) neurons. **a**, Sample traces and raster plots of cell-attached recordings from one ChR2$^+$ (OT$^+$, left) and one ChR2$^-$ (OT$^-$, right) neuron showing reliable activation of ChR2$^+$ (OT$^+$) neurons in response to 50 ms pulses of blue light at 5 Hz (20–100% laser power). **b**, Increase in the number of spikes (left) of ChR2$^+$ (OT$^+$; pink circles; n = 7 neurons, N = 5 dams, p = 0.002, one-way ANOVA) and spike probability (right; p = 0.009) in response to 50 ms light pulse steps. Number of spikes of ChR2$^-$ (OT$^-$; black circles; n = 13, N = 3, p = 0.11) neurons, as well as spike probability (p = 0.13) was not modulated. **c**, Sample traces and raster plots of cell-attached recordings of one ChR2$^+$ (OT$^+$, left) and one ChR2$^-$ (OT$^-$, right). ChR2$^+$ (OT$^+$) neuron was reliably activated in response to 200-ms pulses of blue light (0–100% laser power). **d**, Increase in the number of spikes (left) of ChR2$^+$ (OT$^+$; pink circles; n = 9 neurons, N = 6 dams, p = 0.002, one-way ANOVA) and spike probability (right; p = 0.01) in response to 200 ms light pulse steps. Number of spikes of ChR2$^-$ (OT$^-$; black circles; n = 13, N = 3, p = 0.49) neurons, as well as spike probability (p = 0.62) was not modulated. **e**, Increase in firing rate of ChR2$^+$ (OT$^+$; n = 10 neurons, N = 5 dams, p = 0.0001, one-way ANOVA) but not of ChR2$^-$ (OT$^-$; n = 13, N = 3, p = 0.68) neurons in response to 200 ms light pulse of 100% laser power ('Opto') compared to their baseline firing rate immediately preceding ('Pre') and immediately after ('Post') the light pulse. **f**, Change of firing rate of ChR2$^+$ (OT$^+$; n = 10 neurons, N = 5 dams, p = 0.002, Wilcoxon matched-pairs signed-rank two-tailed test) but not of ChR2$^-$ (OT$^-$; n = 13, N = 3, p = 0.91) neurons in response to 200-ms light pulse of 100% laser power ('Opto') compared to baseline firing immediately preceding the light pulse ('Pre'). **g**, Box plots (showing the median (line), second to third quartiles (box), minimum to maximum (whiskers) of latency to first spike was significantly shorter in ChR2$^+$ (OT$^+$; n = 14 neurons, N = 6 dams, p < 0.0001, Mann–Whitney two-tailed test) compared to ChR2$^-$ (OT$^-$; n = 8, N = 2) neurons in response to 200-ms light pulse of 100% laser power. 'First spike' in ChR2$^-$ (OT$^-$) cells was not light-evoked but occurred spontaneously. Data reported as mean ± s.e.m. *P < 0.05. **P < 0.01.

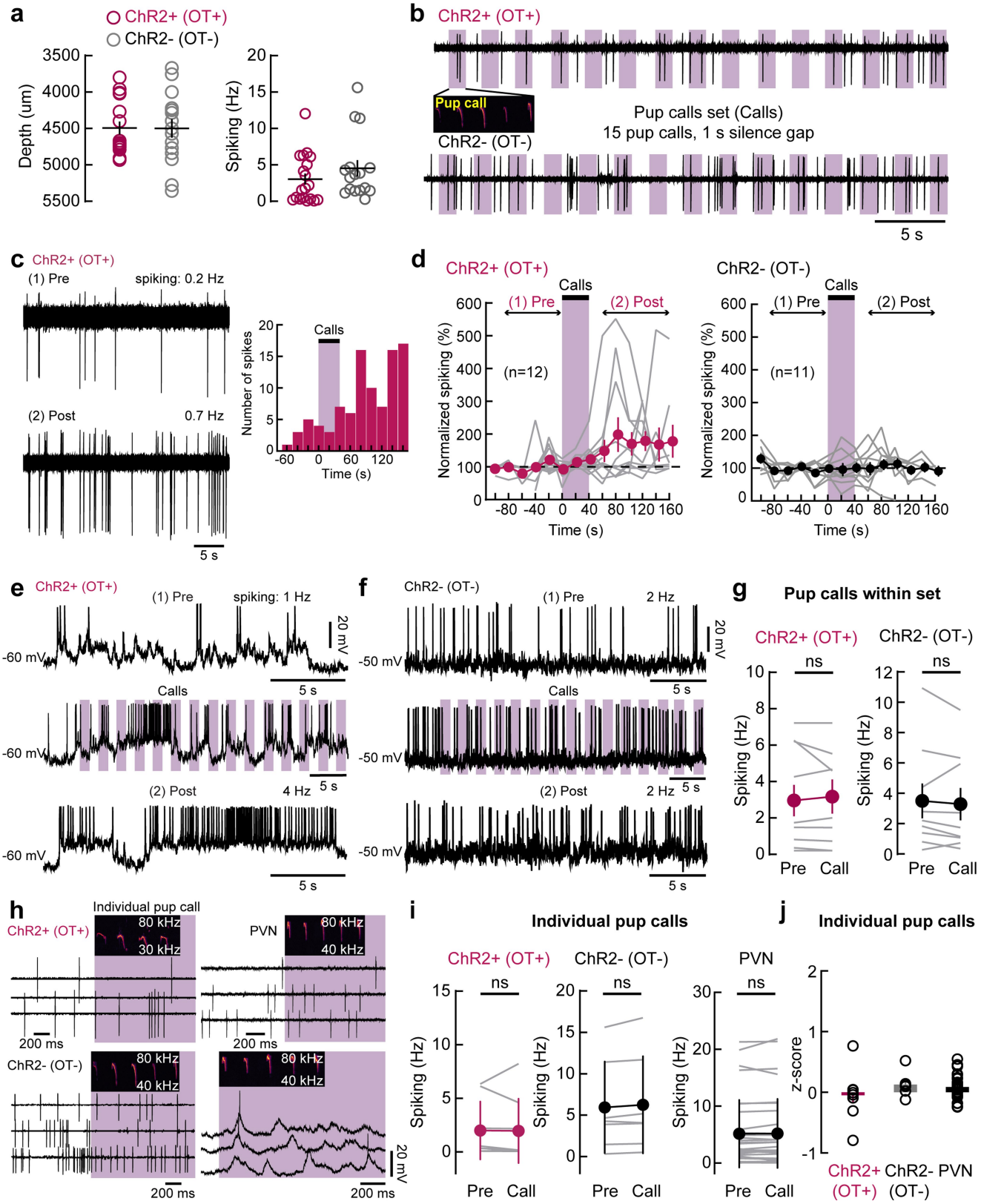

Extended Data Fig. 2 | See next page for caption.

Extended Data Fig. 2 | In vivo responses to individual pup calls. a, Location and firing rate of cell-attached (n = 19 neurons, N = 8 dams) and whole-cell (n = 1) recordings of ChR2$^+$ OT$^+$ neurons and ChR2$^-$ neurons (OT$^-$, cell-attached: n = 16 neurons, N = 8 dams; whole-cell: n = 2, N = 2). **b**, Sample traces of whole-cell recordings of one ChR2$^+$ (OT$^+$; upper trace) and one ChR2$^-$ (OT$^-$; lower trace) neuron during call playback ('Calls'). Pink bars, individual pup calls. **c**, Left, Cell-attached recording of one ChR2$^+$ (OT$^+$) neuron before pup-call onset (1, 'Pre'), and around 2 min after call onset (2, 'Post'). Right, Peristimulus time histogram. Bins: 20 s. **d**, Timeline of ChR2+ (OT$^+$; n = 12 neurons) and ChR2$^-$ (OT$^-$; n = 11) responses. Period before (1, 'Pre') and after (2, 'Post') pup-call onset. **e**,**f**, Sample traces of whole-cell recordings of one ChR2$^+$ (OT$^+$; **e**) and one ChR2$^-$ (OT$^-$; **f**) neuron showing baseline spiking activity preceding onset of pup calls (1, 'Pre', upper trace), activity during playback of a set of pup calls ('Calls', middle trace) and activity after pup calls playback (2, 'Post', lower trace). Note increased firing rate for ChR2$^+$ (OT$^+$) neuron but not ChR2$^-$ (OT$^-$) neuron. **g**, ChR2$^+$ (OT$^+$) did not respond to individual pup calls within a set. 'Pre', average spiking rate of cell-attached recordings during all baseline periods immediately preceding each call within the set. 'Call', average spiking rate during pup-call stimulus for each call within the set. Neither ChR2$^+$ (OT$^+$; n = 9 neurons, N = 6 dams, p = 0.38, Wilcoxon matched-pairs signed-rank two-tailed test), nor ChR2$^-$ (OT$^-$; n = 9, N = 5, p = 0.30) neurons increased their firing rate during individual calls ('Call') compared to baseline ('Pre'). **h**–**j**, ChR2$^+$ (OT$^+$) did not respond to presentation of individual pup calls on a trial-by-trial basis. **h**, Sample traces of cell-attached recordings of one ChR2$^+$ (OT$^+$), one ChR2$^-$ (OT$^-$) and one unidentified PVN neuron, as well as whole-cell recording of a PVN neuron during trial-by-trial individual pup-call presentation. **i**, No increase in the firing rates of either ChR2$^+$ (OT$^+$; n = 8 neurons, N = 2 dams, p = 0.38, Wilcoxon matched-pairs signed-rank two-tailed test), ChR2$^-$ (OT$^-$; n = 7, N = 3, p = 0.08), or unidentified PVN (cell-attached: n = 26, N = 13; whole-cell: n = 6, N = 4, p = 0.48) neurons during individual pup calls ('Call') compared to baseline ('Pre') on a trial-by-trial basis. **j**, No difference in the z-scores of spiking responses of cell-attached and whole-cell recordings during individual pup calls in ChR2$^+$ (OT$^+$; n = 8, N = 2, p = 0.30, one-way ANOVA), ChR2$^-$ (OT$^-$; n = 7, N = 4), and unidentified PVN (cell-attached: n = 21, N = 11; whole-cell: n = 6, N = 4) neurons. Data reported as mean ± s.e.m. *P < 0.05.

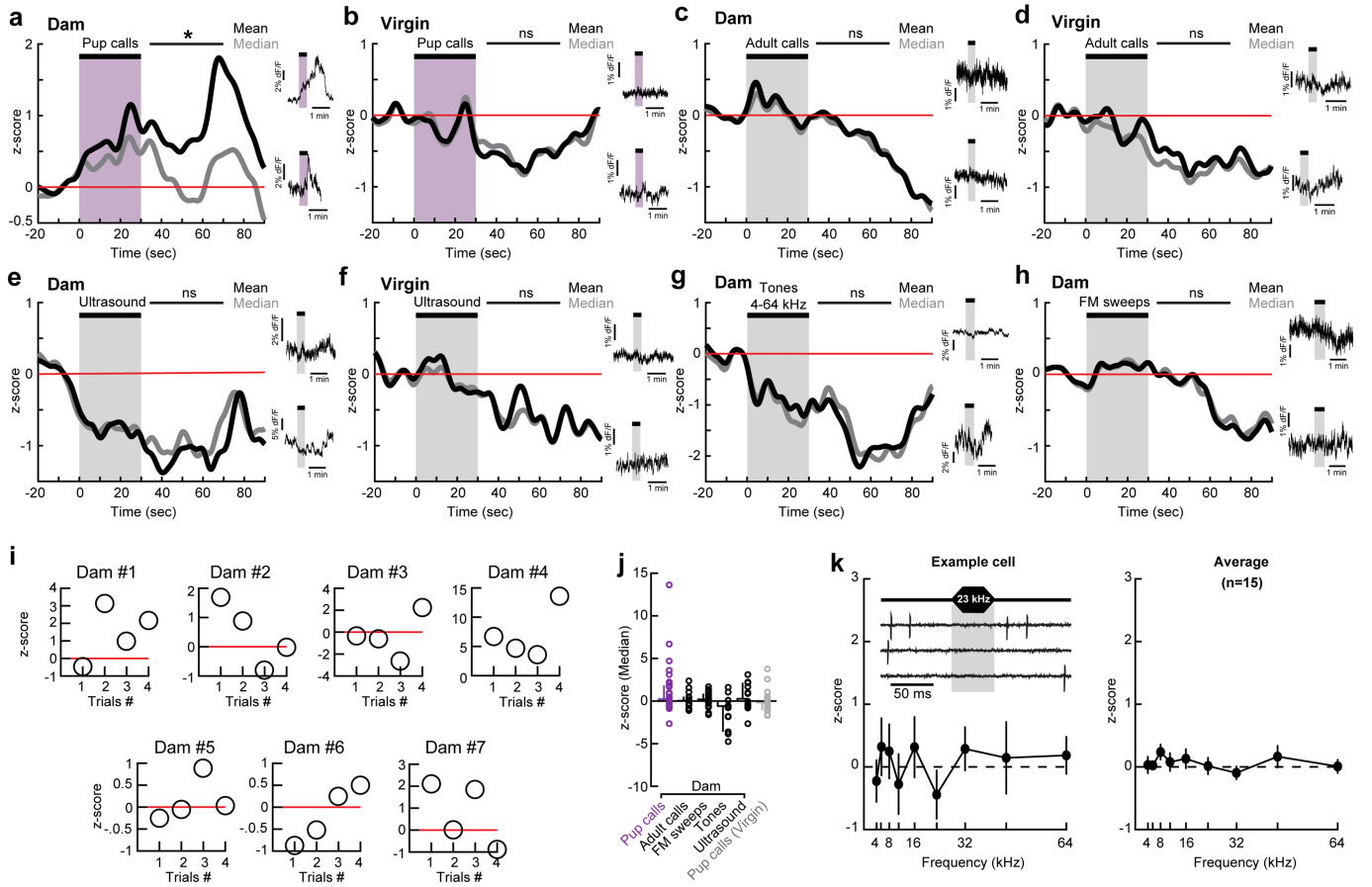

Extended Data Fig. 3 | In vivo responses to auditory stimuli. a–**h**, *Z*-scores of fluorescence activity during fibre photometry recordings of dams and virgins in response to auditory stimuli. Pup calls trigger sustained increase in the activity of oxytocin neurons in dams (**a**; N = 7; Pre vs Post: p = 0.018; Wilcoxon matched-pairs signed-rank one-tailed test) but not virgins (**b**; N = 4; p = 0.50; Wilcoxon matched-pairs signed-rank one-tailed test). No responses to adult calls (**c**; N = 4 dams; p = 0.5966; and **d**; N = 3 virgins; p = 0.09; Wilcoxon matched-pairs signed-rank one-tailed test) or ultrasound pure tones (**e**; N = 3 dams; p = 0.38; and **f**; N = 3 virgins; p = 0.47; Wilcoxon matched-pairs signed-rank one-tailed test). No response to pure tones (**g**; N = 3; p = 0.11; Wilcoxon matched-pairs signed-rank one-tailed test) or FM sweeps (**h**; N = 5; p = 0.20; Wilcoxon matched-pairs signed-rank one-tailed test) in dams. Insets represent fluorescence activity during a single trial from two different mice per condition. **i**, Responses to pup calls across dams and trials (pup calls, dam: n = 28 trials; adult calls, dam: n = 16; FM sweeps, dam: n = 19; tones, dam: n = 12; ultrasound, dam: n = 12; pup calls, virgin: n = 16). **j**, Average z-score responses to auditory stimuli for individual trials. **k**, PVN neurons did not respond to individual pure tones. Left, example cell-attached recording of one PVN neuron in response to 23 kHz tone presentation and tuning profile of pure-tone frequency responses in this cell. Right, average tuning profile of pure-tone frequency responses in PVN cells (n = 15 neurons, N = 9 dams). Data reported as median ± 95% CI (**j**) or as median or mean ± s.e.m. (**k**). **P* < 0.05.

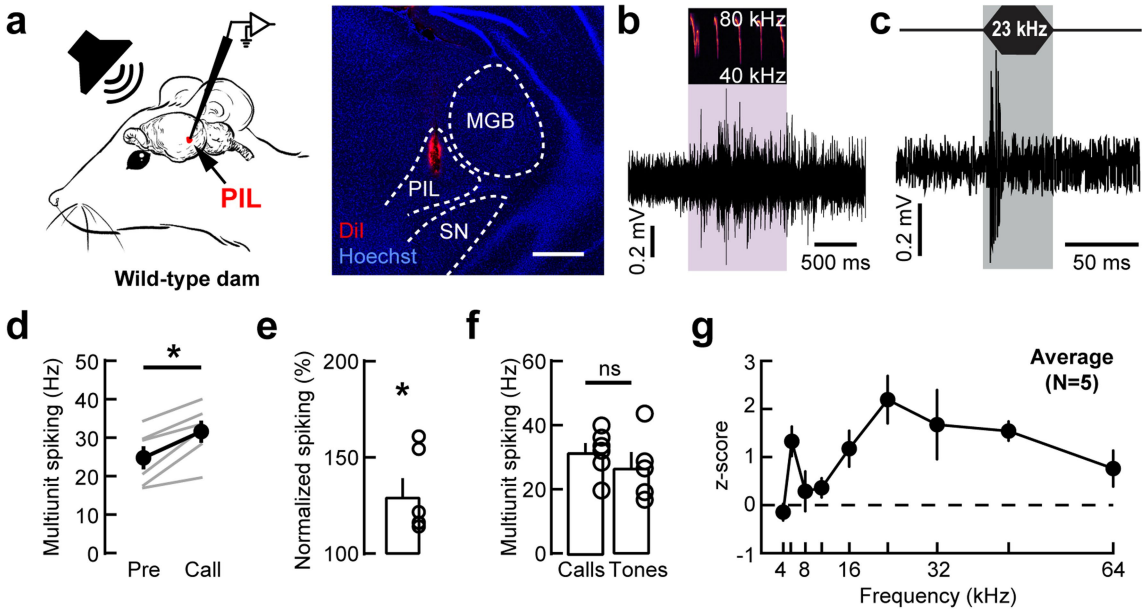

Extended Data Fig. 4 | Auditory responses in the PIL. a, Left, experimental set-up showing in vivo multiunit recordings via tungsten electrode in the PIL of awake head-fixed wild-type dams while playing pup calls from an ultrasound speaker. Right, validation of PIL recording site by coating tungsten electrode tip with DiI. Scale, 500 µm. MGB, medial geniculate body of the thalamus; PIL, posterior intralaminar nucleus of the thalamus; SN, substantia nigra. **b**–**g**, In vivo activation of PIL during playback of pup calls and pure tones. Sample trace of stimulus-evoked PIL multiunit spiking activity during individual pup call (**b**) and 23 kHz tone (**c**) presentation. Note the increase in PIL activity during the entire duration of the pup call (>1 s) compared to transient activation during pure tones. Pup calls increased the firing frequency of PIL neurons (**d**; N = 6 dams, p = 0.03, Wilcoxon matched-pairs signed-rank two-tailed test) which corresponded to a significant increase from baseline values (**e**; N = 6 dams; p = 0.02, one-sample two-tailed Student's *t*-test). **f**, There was no difference in the frequency of multiunit spiking during pup calls and pure tones playback (N = 6 dams; p = 0.33, Mann–Whitney two-tailed test). **g**, Tuning profile of pure-tone frequency responses in PIL (N = 5 dams). Data reported as mean ± s.e.m. *$P < 0.05$; ns, not significant.

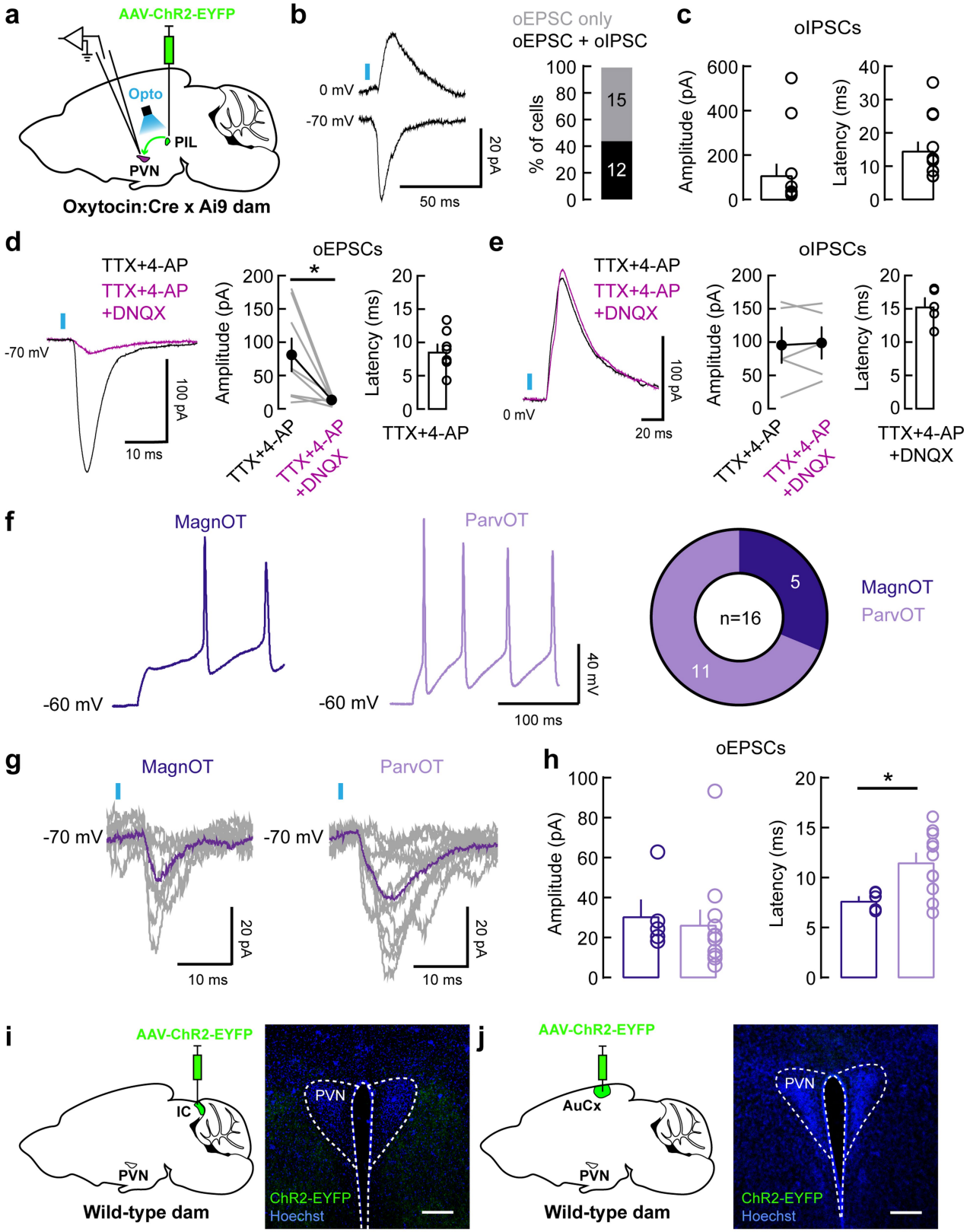

Extended Data Fig. 5 | See next page for caption.

Extended Data Fig. 5 | Auditory projections to the PVN. a, Schematic showing injection of AAV1-hSyn-hChR2(H134R)-EYFP in the PIL of Oxytocin:Cre × Ai9 dams prior to whole-cell recordings from oxytocin neurons (tdTomato$^+$) in PVN brain slices. PIL, posterior intralaminar nucleus of the thalamus; PVN, paraventricular nucleus of the hypothalamus. **b**,**c**, PVN oxytocin neurons receive mainly glutamatergic input from the PIL. Percentage of optogenetically evoked excitatory (oEPSCs) and inhibitory (oIPSCs) currents in oxytocin neurons triggered by optogenetic stimulation of PIL axons (**b**) and characterization of oIPSCs (**c**; n = 12 neurons). **d**,**e**, PIL inputs to oxytocin cells are monosynaptic. **d**, Example traces and summary graph showing oEPSCs in the presence of TTX and 4-AP and their inhibition by DNQX (n = 8 neurons, p = 0.016, Wilcoxon matched-pairs signed-rank test). **e**, Example traces and summary graph showing oIPSCs in the presence of TTX and 4-AP; DNQX had no effect on oIPSCs amplitude (n = 5 neurons, p = 0.63, Wilcoxon). **f**–**h**, Parvocellular PVN oxytocin neurons are the main target of input from the PIL. Magnocellular (MagnOT) and parvocellular (ParvOT) oxytocin neurons were characterized by their signature spiking patterns in current-clamp mode (**f**; left). 5/16 MagnOT and 11/16 ParvOT cells received inputs from the PIL (**f**; right). **g**,**h**, Characterization of oEPSCs in MagnOT and ParvOT neurons triggered by optogenetic stimulation of PIL axons. **g**, Example traces from one magnocellular (left) and one parvocellular (right) oxytocin cell. There was no difference in oEPSCs amplitude (**h**, left; MagnOT: n = 5 neurons, ParvOT: n = 11; p = 0.51, Mann–Whitney two-tailed test) but the latency of oEPSCs in ParvOT cells was longer (**h**, right; MagnOT: n = 5 neurons, ParvOT: n = 11; p = 0.0275, Mann–Whitney two-tailed test). **i**, The PVN does not receive input from IC. Left, injection of AAV1-hSyn-hChR2(H134R)-EYFP in IC of wild-type dams. Right, no EYFP staining was found in PVN, suggesting that IC does not project to PVN. Scale, 200 µm. N = 3. IC, inferior colliculus. **j**, The PVN does not receive input from AuCx. Left, injection of AAV1-hSyn-hChR2(H134R)-EYFP in AuCx of wild-type dams. Right, no EYFP staining was found in PVN, suggesting that AuCx does not project to PVN. Scale, 200 µm. N = 2. AuCx, auditory cortex. Data reported as mean ± s.e.m. *$P < 0.05$.

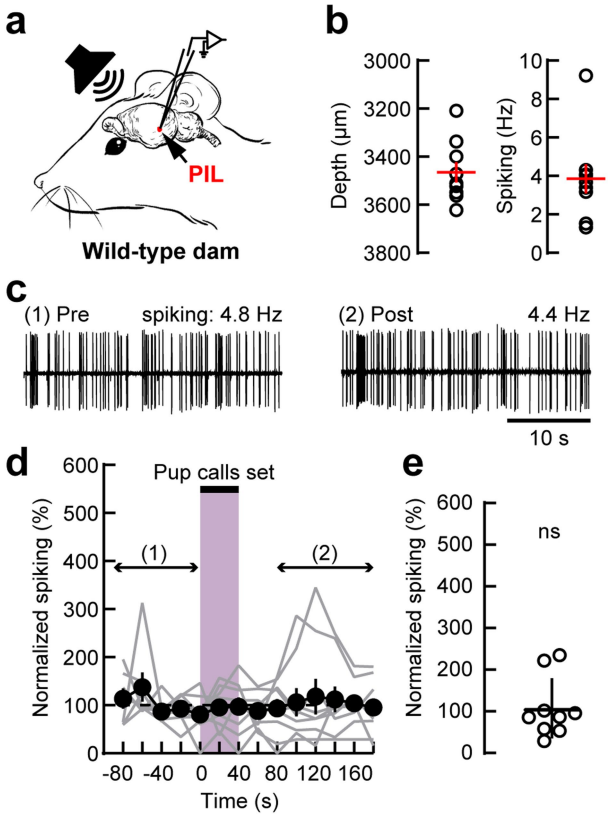

Extended Data Fig. 6 | PIL neurons do not exhibit sustained increases in firing after pup calls in vivo. a, Experimental set-up showing in vivo cell-attached recordings in PIL of awake wild-type dams while playing pup calls from an ultrasound speaker. PIL, posterior intralaminar nucleus of the thalamus. **b**, Location (depth from pia) and firing rate of PIL neurons (n = 9 neurons; N = 4 dams). **c**–**e**, PIL neurons did not modulate their firing rate following playback of a set of pup calls (15 pup calls, 1 s gap in between calls). **c**, Sample traces from a cell-attached recording of one PIL neuron showing its baseline firing rate immediately preceding (1, 'Pre') and at 90 s after the onset of pup calls playback (2, 'Post'). Firing rates during baseline and after pup calls were calculated over 1–2 min. **d**, Timeline of responses of PIL neurons. **e**, PIL neurons (n = 9) did not exhibit persistent increases in baseline firing following pup calls, as calculated between 80–160 s after onset of pup-call playback (**e**, n = 9 neurons, N = 4 dams, p = 0.77, one-sample two-tailed Student's *t*-test). Data reported as mean ± s.e.m.; ns, not significant.

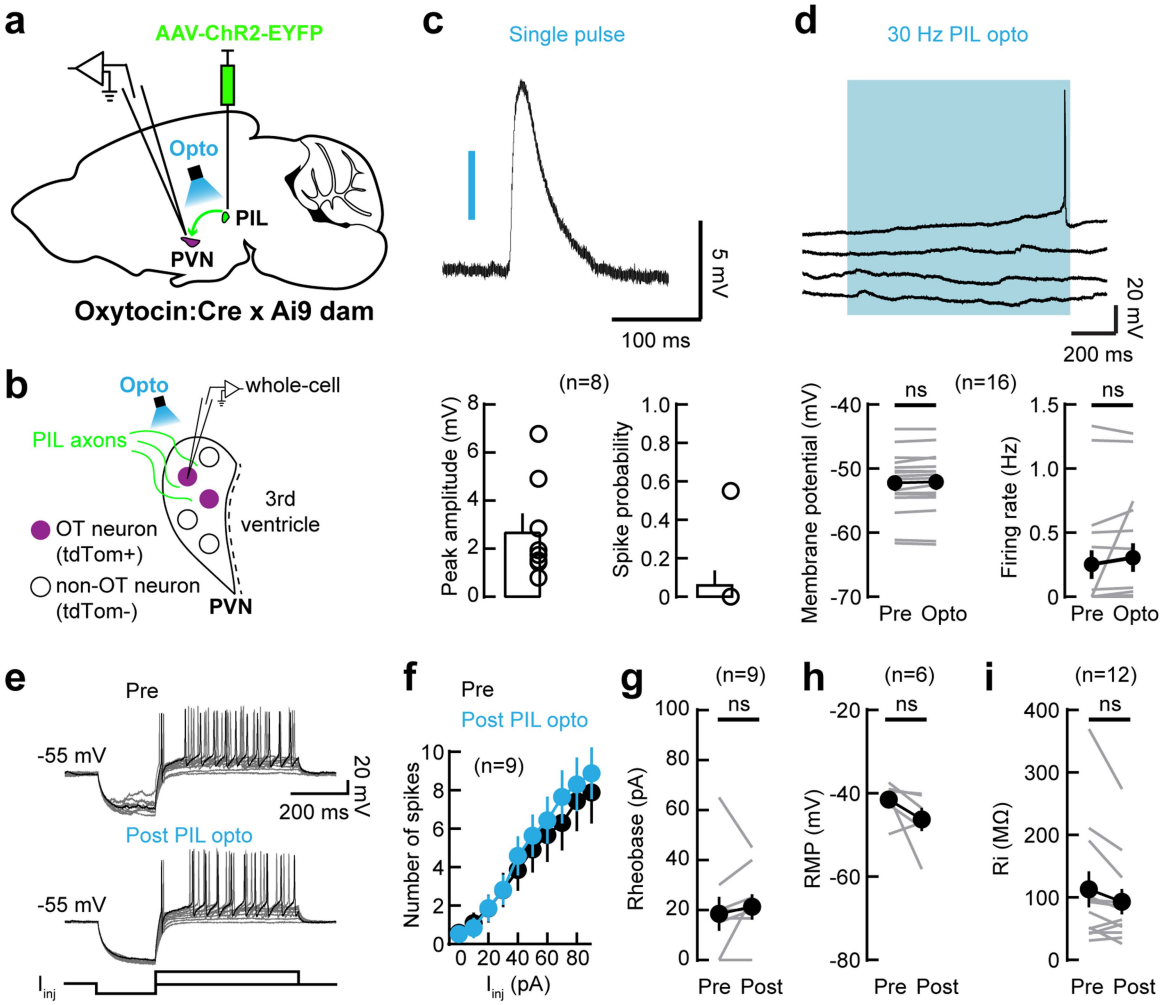

Extended Data Fig. 7 | PIL inputs to the PVN do not induce postsynaptic spiking or affect the excitability of oxytocin neurons. a, Schematic showing injection of AAV1-hSyn-hChR2(H134R)-EYFP in PIL of Oxytocin:Cre × Ai9 dams before whole-cell recordings from oxytocin neurons (tdTomato$^+$) in PVN brain slices. PIL, posterior intralaminar nucleus of the thalamus; PVN, paraventricular nucleus of the hypothalamus. **b**, Whole-cell recordings from tdTomato+ oxytocin neurons in PVN slices, optogenetic stimulation of PIL axons and placement of the extracellular stimulation electrode. **c**,**d**, Optogenetic stimulation of PIL axons in PVN does not induce postsynaptic spiking in oxytocin neurons. **c**, Single pulse of optogenetic stimulation triggered postsynaptic potentials but did not induce spiking in oxytocin cells (n = 8 neurons). **d**, Repeated optogenetic stimulation of PIL axons ('PIL opto') did not trigger depolarization of oxytocin cells (n = 16 neurons; p = 0.10, Wilcoxon matched-pairs signed-rank two-tailed test) and did not induce postsynaptic spiking (n = 16 neurons; p = 0.26, Wilcoxon matched-pairs signed-rank two-tailed test). **e**,**f**, No change in the number of spikes in oxytocin neurons in response to 20 pA steps of intracellular current injection before ('Pre') or after ('Post') PIL opto. Sample traces (**e**) and summary (**f**; n = 9 neurons, p > 0.44, Wilcoxon matched-pairs signed-rank two-tailed test). **g**–**i**, No change in the intrinsic properties of oxytocin neurons after PIL opto, in terms of rheobase (**g**; n = 9 neurons; p = 0.38, Wilcoxon matched-pairs signed-rank two-tailed test), resting membrane potential (**h**; n = 6 neurons; p = 0.16, Wilcoxon matched-pairs signed-rank two-tailed test), or input resistance (**i**; n = 12 neurons; p = 0.06, Wilcoxon matched-pairs signed-rank two-tailed test). Data reported as mean ± s.e.m.

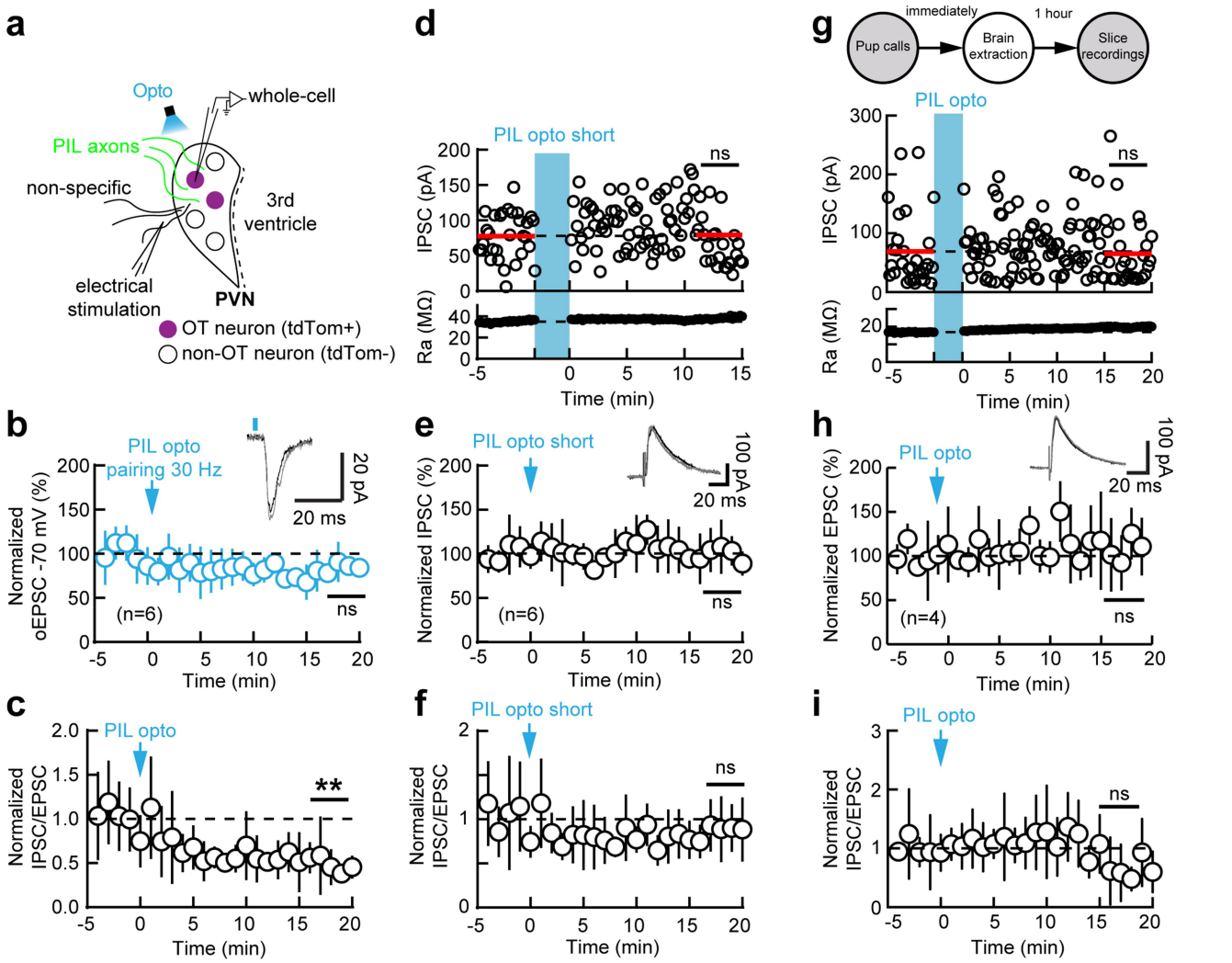

Extended Data Fig. 8 | Prolonged but not brief optogenetic stimulation of PIL axons triggers iLTD. a, Whole-cell recordings from tdTomato$^+$ oxytocin neurons in PVN slices, optogenetic stimulation of PIL axons and placement of the extracellular stimulation electrode. **b**, Whole-cell voltage-clamp recordings showing that the amplitude of oEPSCs triggered by single pulse of optogenetic stimulation was not modified following repeated optogenetic stimulation of PIL axons ('PIL opto'; n = 6 neurons, p = 0.13, one-sample two-tailed Student's *t*-test). **c**, IPSC/EPSC ratio decreased following PIL opto (n = 6 neurons; p = 0.0018, one-sample two-tailed Student's t-test). **d**–**f**, Repeated but brief optogenetic stimulation of PIL axons ('PIL opto short') did not induce iLTD: example cell (**d**; p = 0.74, Mann–Whitney two-tailed test) and summary (**e**; n = 6 neurons, p = 0.99, one-sample two-tailed Student's t-test). **f**, No change in IPSC/EPSC ratio following PIL opto short (n = 6 neurons; p = 0.49, one-sample two-tailed Student's t-test). **g**–**i**, In vivo exposed to pup calls playback occlude iLTD. **g**,**h**, Schematic of experimental protocol (**g**): example cell (**g**; p = 0.94, Mann–Whitney two-tailed test) and summary (**h**; n = 4 neurons, p = 0.98, one-sample two-tailed Student's *t*-test). **i**, No change in IPSC/EPSC ratio following PIL opto in slices of dams exposed to pup calls in vivo (n = 4 neurons; p = 0.76, one-sample two-tailed Student's *t*-test). Data reported as mean ± s.d. $^{**}P < 0.01$; ns, not significant.

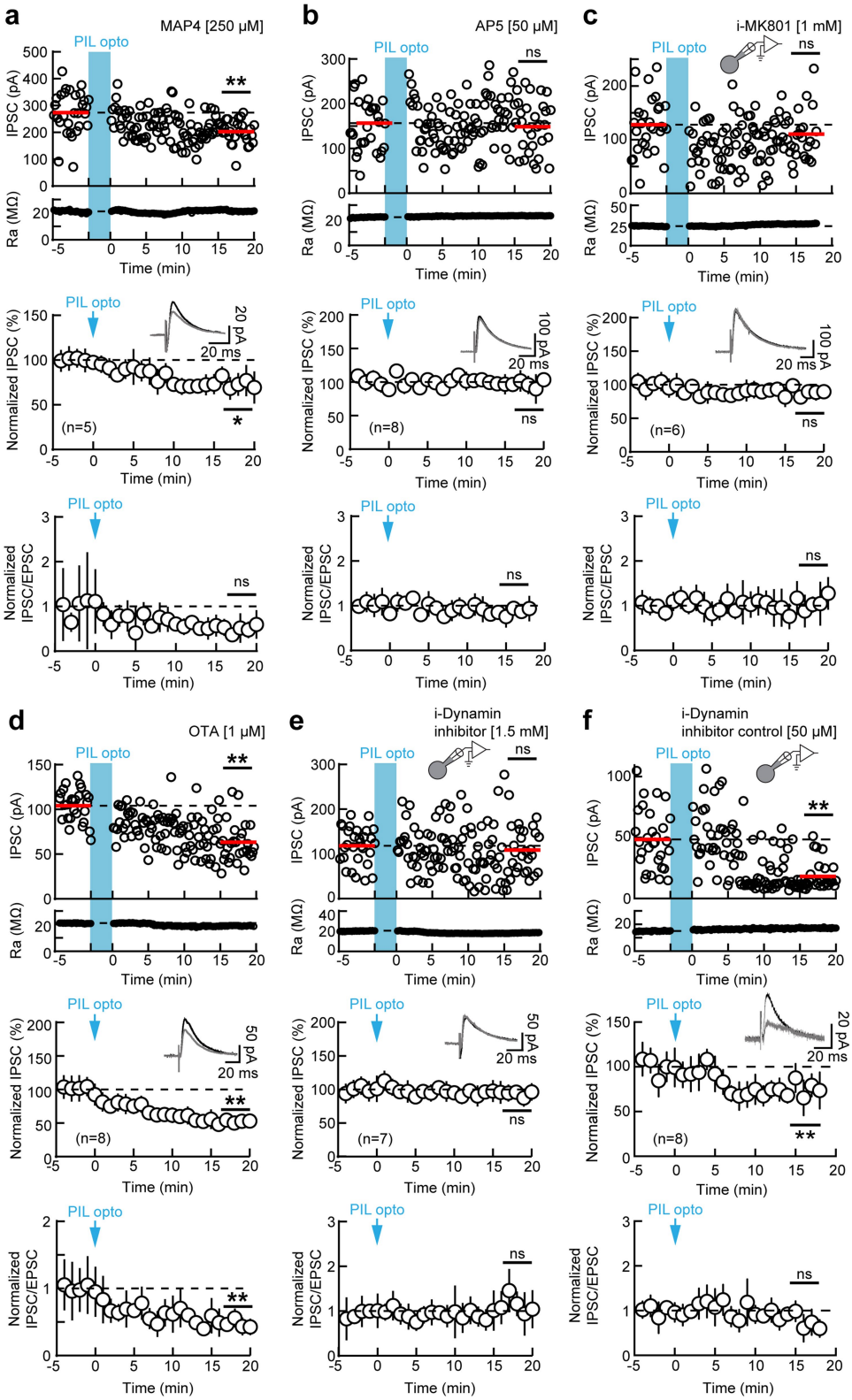

Extended Data Fig. 9 | See next page for caption.

Extended Data Fig. 9 | iLTD in oxytocin neurons relies on postsynaptic NMDARs and dynamin signalling. a, Whole-cell voltage-clamp recordings showing intact iLTD after repeated optogenetic stimulation of PIL terminals in PVN ('PIL opto') in presence of bath-applied type-III mGluR antagonist MAP4 (250 μM), for example neuron (top; $p < 0.0001$, Mann–Whitney two-tailed test) and summary (middle; n = 5 neurons, $p = 0.02$, one-sample two-tailed Student's *t*-test). Bottom, IPSC/EPSC ratio in the presence of MAP4. **b**, iLTD in oxytocin neurons is NMDAR-dependent. Whole-cell voltage-clamp recordings showing no plasticity after PIL opto in presence of bath-applied AP5 (50 μM), for example neuron (top; $p = 0.62$, Mann–Whitney two-tailed test) and summary (middle; n = 8 neurons, $p = 0.44$, one-sample two-tailed Student's *t*-test). Bottom, unchanged IPSC/EPSC ratio in the presence of AP5. **c**, iLTD in oxytocin neurons is dependent on postsynaptic NMDARs. Whole-cell voltage-clamp recordings showing no plasticity after PIL opto when i-MK801 (1 mM) was applied in the recording pipette, for example neuron (top; $p = 0.11$, Mann–Whitney two-tailed test) and summary (middle; n = 6 neurons, $p = 0.18$, one-sample two-tailed Student's *t*-test). Bottom, unchanged IPSC/EPSC ratio in the presence of i-MK801. **d**, Whole-cell voltage-clamp recordings showing intact iLTD after PIL opto in presence of bath-applied OXTR antagonist OTA (1 μM), for example neuron (top; $p < 0.0001$, Mann–Whitney two-tailed test) and summary (middle; n = 8 neurons, $p = 0.0008$, one-sample two-tailed Student's *t*-test). Bottom, IPSC/EPSC ratio in the presence of OTA. **e**,**f**, iLTD in oxytocin neurons is dependent on dynamin signalling. **e**, Whole-cell voltage-clamp recordings showing no plasticity after PIL opto when i-Dynamin inhibitor (1.5 mM) was applied in the recording pipette, for example neuron (top; $p = 0.30$, Mann–Whitney two-tailed test) and summary (middle; n = 7 neurons, $p = 0.63$, one-sample two-tailed Student's *t*-test). Bottom, unchanged IPSC/EPSC ratio in the presence of i-Dynamin inhibitor. **f**, Whole-cell voltage-clamp recordings showing intact iLTD in oxytocin cells in the presence of a scrambled dynamin inhibitor in the recording pipette, for example neuron (top; $p < 0.0001$, Mann–Whitney two-tailed test) and summary (middle; n = 8 neurons, $p = 0.0096$, one-sample two-tailed Student's *t*-test). Bottom, IPSC/EPSC ratio in the presence of a scrambled dynamin inhibitor. Data reported as mean ± s.d. $^{*}P < 0.05$, $^{**}P < 0.01$; ns, not significant.

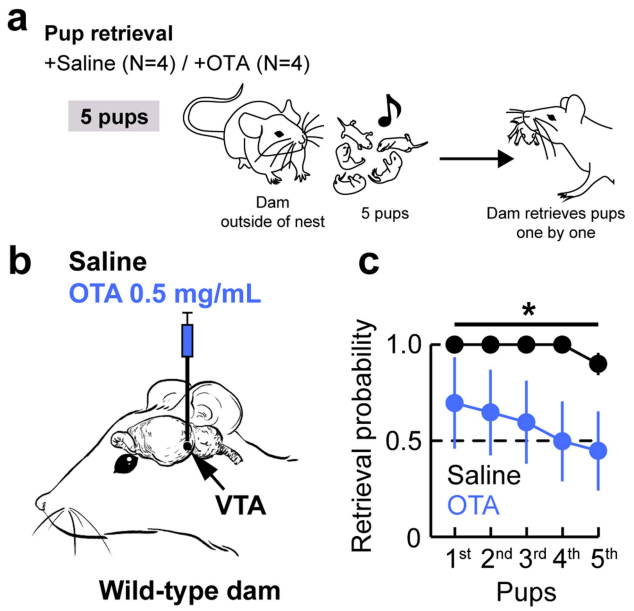

Extended Data Fig. 10 | Inhibiting oxytocin signalling in the VTA impairs pup-retrieval behaviour. a, Pup-retrieval protocol. **b**,**c**, Wild-type dams infused with the OXTR antagonist OTA (0.5 mg ml^{-1}; **b**) retrieved less pups compared to saline controls (**c**; N = 4 dams, *P* at least <0.02, two-tailed Fisher's test). Data reported as mean ± s.e.m. *$P < 0.05$.

nature portfolio

Corresponding author(s): Silvana Valtcheva, Robert C. Froemke

Last updated by author(s): Jun 23, 2023

Reporting Summary

Nature Portfolio wishes to improve the reproducibility of the work that we publish. This form provides structure for consistency and transparency in reporting. For further information on Nature Portfolio policies, see our Editorial Policies and the Editorial Policy Checklist.

Statistics

For all statistical analyses, confirm that the following items are present in the figure legend, table legend, main text, or Methods section.

n/a	Confirmed
☐	☒ The exact sample size (*n*) for each experimental group/condition, given as a discrete number and unit of measurement
☐	☒ A statement on whether measurements were taken from distinct samples or whether the same sample was measured repeatedly
☐	☒ The statistical test(s) used AND whether they are one- or two-sided *Only common tests should be described solely by name; describe more complex techniques in the Methods section.*
☒	☐ A description of all covariates tested
☐	☒ A description of any assumptions or corrections, such as tests of normality and adjustment for multiple comparisons
☐	☒ A full description of the statistical parameters including central tendency (e.g. means) or other basic estimates (e.g. regression coefficient) AND variation (e.g. standard deviation) or associated estimates of uncertainty (e.g. confidence intervals)
☐	☒ For null hypothesis testing, the test statistic (e.g. *F*, *t*, *r*) with confidence intervals, effect sizes, degrees of freedom and *P* value noted *Give P values as exact values whenever suitable.*
☒	☐ For Bayesian analysis, information on the choice of priors and Markov chain Monte Carlo settings
☒	☐ For hierarchical and complex designs, identification of the appropriate level for tests and full reporting of outcomes
☒	☐ Estimates of effect sizes (e.g. Cohen's *d*, Pearson's *r*), indicating how they were calculated

Our web collection on statistics for biologists contains articles on many of the points above.

Software and code

Policy information about availability of computer code

Data collection	Clampex 10.7 (Molecular Devices), Avisoft-SASLab Pro (Avisoft-Bioacoustics), Active X Software (TDT), Synapse Software (TDT), LSM 700 confocal microscope software (Carl Zeiss)
Data analysis	Clampfit 10.7 (Molecular Devices), ImageJ 1.53t (NIH), MATLAB 2020b (MathWorks), Prism 9.5.1 (GraphPad), Adobe Audition 23.3 (Adobe); Scripts used to analyze fiber photometry is available on GitHub: https://github.com/valtchevas/valtcheva_et_al_2023

For manuscripts utilizing custom algorithms or software that are central to the research but not yet described in published literature, software must be made available to editors and reviewers. We strongly encourage code deposition in a community repository (e.g. GitHub). See the Nature Portfolio guidelines for submitting code & software for further information.

Data

Policy information about availability of data

All manuscripts must include a data availability statement. This statement should provide the following information, where applicable:

- Accession codes, unique identifiers, or web links for publicly available datasets
- A description of any restrictions on data availability
- For clinical datasets or third party data, please ensure that the statement adheres to our policy

Information about resources, reagents used, and requests for data should be directed to and will be fulfilled by the Lead Contact, Silvana Valtcheva (silvana.valtcheva@uk-koeln.de) and Robert C. Froemke (robert.froemke@med.nyu.edu).

Field-specific reporting

Please select the one below that is the best fit for your research. If you are not sure, read the appropriate sections before making your selection.

☒ Life sciences ☐ Behavioural & social sciences ☐ Ecological, evolutionary & environmental sciences

For a reference copy of the document with all sections, see nature.com/documents/nr-reporting-summary-flat.pdf

Life sciences study design

All studies must disclose on these points even when the disclosure is negative.

Sample size	No statistical methods were used to predetermine sample size. The experiments were not randomized. Sample sizes were chosen to reliably measure experimental effects while minimizing the number of animals used in accordance with ethical guidelines. Our sample sizes are comparable to those included in previous studies (Schiavo et al., 2020; Carcea et al., 2021; Mei et al., 2023), and were considered appropriate based on the size and statistical significance of the effects and consistency across animals.
Data exclusions	Whole-cell recordings were excluded from analysis if the access resistance changed >30% compared to baseline. Dams which retrieved pups with less than 90% accuracy under saline conditions were excluded.
Replication	Data were collected in an interleaved fashion. In vivo cell-attached and whole-cell channelrhodopsin2-assisted recordings were replicated across neurons and animals PVN (n=38 neurons, N=17 animals). In vivo cell-attached and whole-cell blind recordings were replicated across neurons and animals for both PVN (n=23, N=17) and PIL (n=9, N=4). Tungsten recordings in PIL were replicated across recording sites and animals (N=6). Fiber photometry recordings were replicated across recording sites and animals for both dams (N=16) and virgins (N=11). In vitro slice recordings were replicated across neurons and animals: ChR2-assisted circuit mapping (IC to PIL, n=12, N=3; AuCx to PIL, n=13, N=2; PIL to PVN, n=67, N=12). Transmission experiments (PIL opto oEPSCs/oIPSCs,n=27, N=7; TTX+4-AP, n=8, N=2; PIL opto MagnOT/ParvOT, n=16, N=7; NMDAR currents, n=7, N=2; PIL +CNO, n=6, N=2; PIL opto single, n=8, N=2; PIL opto 30Hz, n=16, N=7). Long-term plasticity experiments (PIL opto spiking, n=9, N=3; PIL opto, n=10, N=6; PIL opto oEPSCs, n=6, N=2; PIL opto short, n=6, N=3; Occlusion, n=4, N=2; MAP4, n=5, N=2; AP5, n=8, N=4; MK-801 n=6, N=4; OTA, n=8, N=4; i-Dynamin inh, n=7, N=3; i-Dynamin inh ctr, n=8, N=4). Excitability experiments (n=9, N=4). Intrinsic properties experiments (n=12, N=8). Behavior experiments were replicated across animals for both chemogenetic inhibition (speaker approach test: N=4; pup retrieval test: N=27) and cannula infusion (N=4). Oxytocin sensor experiments were replicated across animals (blue light+pup calls, N=5; blue light+tones, N=4; blue light only, N=5; blue light +pup calls+CNO, N=4). Tracing experiments: Rabies virus (N=4), IC to PVN (N=3), AuCx to PVN (N=2), Oxytocin fibers in VTA (N=2).
Randomization	Animals were randomly assigned to different groups.
Blinding	The investigators were blinded to allocation during behavioral testing, fiber photometry data analysis and oxytocin sensor data analysis. Blinding was not relevant and not performed for in vivo cell-attached, whole-cell and tungsten recordings, fiber photometry experiments, oxytocin sensor experiments, in vitro whole-cell recordings due to the fact that auditory stimuli/optogenetic stimulation in vivo, and optogenetic/electrical stimulation and/or pharmacological application in vitro were performed in real-time by the experimenter. Blinding was not relevant and not performed for data analysis of in vivo cell-attached, whole-cell and tungsten recordings, as well as for in vitro whole-cell recordings due to the fact that data analysis was performed in real-time by the experimenter.

Reporting for specific materials, systems and methods

We require information from authors about some types of materials, experimental systems and methods used in many studies. Here, indicate whether each material, system or method listed is relevant to your study. If you are not sure if a list item applies to your research, read the appropriate section before selecting a response.

Materials & experimental systems

n/a	Involved in the study
☐	☒ Antibodies
☒	☐ Eukaryotic cell lines
☒	☐ Palaeontology and archaeology
☐	☒ Animals and other organisms
☒	☐ Human research participants
☒	☐ Clinical data
☒	☐ Dual use research of concern

Methods

n/a	Involved in the study
☒	☐ ChIP-seq
☒	☐ Flow cytometry
☒	☐ MRI-based neuroimaging

Antibodies

Antibodies used

Primary antibodies: GFP Tag Polyclonal Antibody (Thermo Fisher Scientific, Item# A10262), Anti-mCherry antibody (Abcam, Item# ab167453), Anti-Oxytocin Antibody (Millipore Sigma, Item# AB911). Secondary antibodies: Goat anti-Rabbit IgG (H+L) Cross-Adsorbed Secondary Antibody, Alexa Fluor 555 (Thermo Fisher Scientific, Item# A-21428), Goat anti-Chicken IgY (H+L) Secondary Antibody, Alexa Fluor 488 (Thermo Fisher Scientific, Item# A-11039).

Validation

All antibodies were validated for use in fixed sections of mouse brain.

GFP Tag Polyclonal Antibody (Thermo Fisher Scientific, Item# A10262) - Application: Western Blot, Immunocytochemistry. Citation: Sunico et al., (2010) J Neurosci. Jan 20;30(3):973-84.

Anti-mCherry antibody (Abcam, Item# ab167453) - Application: Western Blot, Immunocytochemistry. Citation: Kumar et al., (2022) Nat Commun. Feb 21;13(1):974.

Anti-Oxytocin Antibody (Millipore Sigma, Item# AB911) - Application: Dot Blot, Immunocytochemistry, Radioimmunoassay. Citation: Carcea et al., (2021) Nature. Aug;596(7873):553-557.

Animals and other organisms

Policy information about studies involving animals; ARRIVE guidelines recommended for reporting animal research

Laboratory animals

Wild-type C57BL/6N (Taconic, B6-F) female maternal mice (dams) were used for in vivo and in vitro electrophysiology, anatomy tracings, oxytocin sensor experiments and behavior. Oxytocin:Cre (Jackson, 024234) female maternal mice (dams) were used for anatomy tracings and fiber photometry. Oxytocin:Cre x Ai9 female maternal mice (dams) were used for in vitro electrophysiology and anatomy tracings. Oxytocin:Cre x Ai32 female maternal mice (dams) were used for in vivo electrophysiology and histology validation. All animals were bred on C57BL/6N background. All animals were at least 3 months old at time of experiments. Animals were housed at ~22°C, relative humidity of ~45%. Light cycle was 12 hour on/off cycle (6:30 AM - 6:30 PM light)

Wild animals

No wild animals were used in this study.

Field-collected samples

No field samples were collected for this study.

Ethics oversight

All procedures were approved under NYU School of Medicine IACUC protocols, in accordance with NIH guidelines. Animals were housed in fully-equipped facilities in the NYU School of Medicine Science Building (New York City). The facilities were operated by the NYU Division of Comparative Medicine.

Note that full information on the approval of the study protocol must also be provided in the manuscript.